



1 **Review Article: Rainfall-Induced Landslide Prediction Models, Part I: Empirical-**

2 **Statistical and Physically Based Causative Thresholds**

3 Kyrillos M.P. Ebrahim^{1,2}, Sherif M.M.H. Gomaa^{1,2}, Tarek Zayed¹, Ghasan Alfalah³

4

5 ¹Department of Building and Real Estate, Faculty of Construction and Environment, The Hong
6 Kong Polytechnic University, Hung Hom, Kowloon, Hong Kong SAR.

7 ²Structural Engineering Department, Faculty of Engineering, Mansoura University, Mansoura,
8 Egypt.

9 ³Department of Architecture and Building Sciences, King Saud University, Riyadh, Saudi
10 Arabia

11

12 Correspondence to: Kyrillos M.P. Ebrahim (kyrillos.ebrahim@connect.polyu.hk), Sherif
13 M.M.H. Gomaa (sherif.gomaa@polyu.edu.hk), Ghasan Alfalah (galfalah@ksu.edu.sa)

14



15 **ABSTRACT.**

16 Landslides rank among the most devastating hazards, leading to loss of life and destruction of
17 infrastructure, with rainfall being a primary triggering factor. Global climate change has
18 increased landslide occurrence; accordingly, accurate landslide prediction is crucial to
19 reduce damage and losses. Since landslides account for 17% of all natural hazard fatalities,
20 several studies have been done across the globe to predict these events better. Despite the
21 considerable number of review articles, a comprehensive comparison between empirically,
22 physically, deterministically, and phenomenologically based prediction models is still missing.
23 Moreover, they lack adopting mixed methodology. Accordingly, a mixed review that comprised
24 scientometric, systematic, and bibliometric analysis was employed. This study (Part I of a two-
25 part review) examines two approaches for analyzing local-scale landslides: empirical-statistical
26 methods and physically based causative threshold models. Deterministic and
27 phenomenologically based prediction models are discussed in part ii and have been published
28 (Ebrahim et al., 2024a). This study explores the practicality and constraints associated with the
29 aforementioned methodologies. As a result, critical insights into rainfall-induced landslides are
30 examined. Macroscopically, antecedent rainfall surpasses the intensity-duration thresholds.
31 Physically based causative thresholds can be utilized when geotechnical or hydrological data
32 are limited. Microscopely, hybrid artificial intelligence models provide higher prediction
33 accuracies. Finally, research suggestions are highlighted, as modeling artificial intelligence
34 models with extensive datasets to achieve high prediction accuracy is still needed for further
35 development.

36 **Keywords:** Landslides; Prediction; Rainfall-induced landslides; Empirical models; Physically-
37 based models.

38



39 **INTRODUCTION.**

40 “A landslide is the movement of a mass of rock, earth, or debris down a slope (Cruden, 1991).”

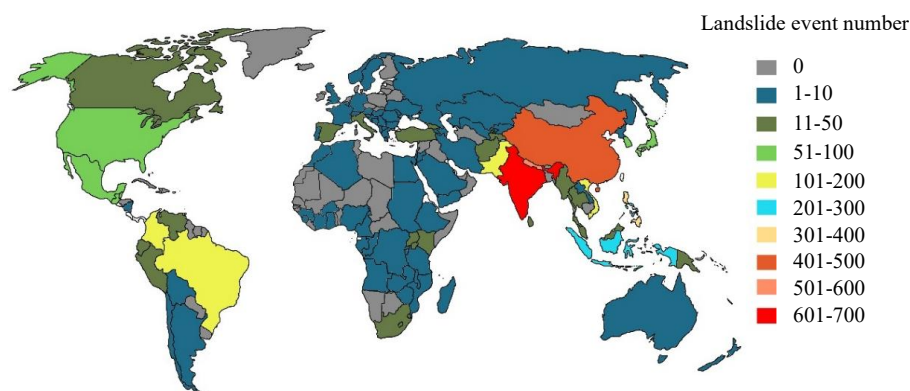
41 These events naturally occur in hilly regions and play an essential role in shaping mountainous
42 landscapes. Landslides happen when the strength of rock or soil is insufficient to resist the
43 stresses induced by triggering factors. They are a prevalent hazard in sloped terrains, leading
44 to loss of life, infrastructure destruction, and economic damages (Chae et al., 2020). As
45 illustrated in Figure 1, between January 2004 and December 2016, non-seismic landslides
46 caused the deaths of nearly 55,997 individuals in 4,862 incidents (Froude & Petley, 2018).
47 Additionally, the World Health Organization reported that landslides claimed over 18,000 lives
48 between 1998 and 2017 (Online: Landslides (who. int), accessed October 19, 2024)

49 Landslides can be triggered by various factors, including earthquakes, volcanic activity,
50 floods, and intense rainfall, with rainfall being the most common cause of slope instability.
51 Increasingly severe rainstorms, driven by climate change, are contributing to the occurrence of
52 catastrophic landslides (Zhao et al., 2019a; Wu et al., 2020; Harsa et al., 2023). Hungr et al.
53 (2014) classified landslides into 32 distinct types based on material composition (such as rock,
54 debris, or soil) and movement mechanisms (such as falls, topples, slides, and flows). This
55 classification, an extension of the earlier Varnes system, offers a more comprehensive
56 framework for analyzing landslide processes. By categorizing landslides according to their
57 triggers and dynamics, the classification provides a valuable tool for understanding their
58 complexity. However, this study focuses specifically on rainfall-induced landslides, as they are
59 among the most frequent and destructive types in certain regions.

60 Rain-induced landslides are typically shallow, with slip surfaces running parallel to the
61 slope surface (Saadatkhah et al., 2015; Das et al., 2022; Thang et al., 2022). According to Caine
62 (1980), the depth of shallow landslides is generally less than 2 to 3 meters. Similarly, studies
63 by Zhang et al. (2011) and Huang et al. (2015) reported shallow landslides with a thickness of



64 less than 3 to 5 meters. A ground survey conducted by the Geotechnical Engineering Office
65 (GEO) in Hong Kong identified several shallow landslide scars with vertical depths of under 3
66 meters (Liu et al., 2022). Shallow landslides are particularly hazardous due to their rapid onset
67 and intensity (Formetta & Capparelli, 2019). They involve the movement of soil or debris near
68 the surface, typically extending to depths of only a few meters. In contrast, deep-seated
69 landslides affect larger masses of material, including bedrock, and occur at much greater
70 depths. Figure 2 provides a visual comparison of shallow and deep-seated landslides,
71 highlighting differences in failure depth and material displacement, which are essential to this
72 study's focus (Dou et al., 2015).



73

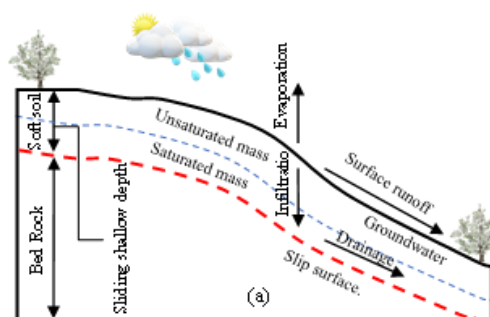
74 **Figure 1.** Fatal non-seismic landslides by nation from 2004 to 2016: Figure reproduced with
75 permission (Froude & Petley, 2018).

76 According to Terzaghi, when a slope experiences movement, any intervention aimed at
77 preventing further sliding must be tailored to the specific mechanisms that initiated the event.
78 Mitigation techniques such as stabilizing piles, soil nailing, drainage systems, and other
79 strategies are crucial, particularly when the slope is exposed to unforeseen triggers like heavy
80 rainfall, earthquakes, or degradation of geotechnical properties (Huang & He, 2023). In recent
81 years, there has been an increased focus on leveraging landslide prediction models to reduce
82 the risks associated with these disasters. These models play a key role in minimizing the

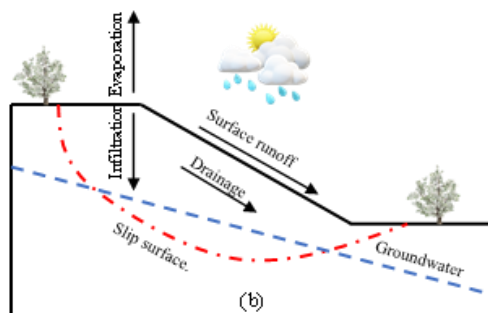


83 impacts of rainfall-induced landslides and facilitating the development of early warning
84 systems (Liang & Uchida, 2022). Landslide prediction models are vital for several reasons.
85 First, they help identify areas prone to landslides, enabling proactive risk mitigation strategies
86 such as constructing retaining walls or planting vegetation. Second, they provide timely alerts
87 of potential landslides, allowing authorities to secure structures and evacuate residents, which
88 can significantly reduce the risk of casualties and property damage. The prediction of landslides
89 has garnered significant attention as a practical approach to forecasting both the spatial
90 (location) and temporal (timing) aspects of landslide events (Valentino et al., 2014; Ma et al.,
91 2017). Therefore, this paper aims to explore the key factors that influence rainfall-triggered
92 landslides, highlighting the importance of each factor in achieving accurate predictions of these
93 events.

94



95



96 **Figure 2.** a) Shallow landslides; b) Deep-seated landslides. (Refer to Hungr et al. (2014) for

97 more information regarding different classifications of landslides)



98 This study will utilize both quantitative (scientometric) and qualitative (systematic)
99 approaches to analyze the existing literature. It will present a range of methods for landslide
100 prediction, including empirical-statistical thresholds, physically based causative models,
101 physical analytical and numerical models, and landslide susceptibility analysis, organized into
102 two distinct sections. This review paper represents the first of two parts, concentrating on
103 rainfall-induced landslide prediction models. This review paper is the first of two parts focused
104 on rainfall-induced landslide prediction models. In this first part, we comprehensively review
105 empirical and physically-based models used to predict rainfall-triggered landslides. The second
106 part of the review has already been published (Ebrahim et al., 2024a) and addresses
107 deterministic models and landslide susceptibility assessments. Together, these two parts offer
108 a complete overview of the different approaches for predicting rainfall-induced landslides,
109 bridging the gap between empirical studies and advanced deterministic modeling techniques.

110 This study integrates various statistical methods, such as statistical regression, artificial
111 intelligence, probabilistic models, and mathematical analytical models, into landslide
112 prediction. It uses bibliometric analysis to assess and evaluate the accuracy of these statistical
113 models. Part II of the study provides a detailed theoretical framework for rainfall-induced
114 landslides and their initial conditions, as outlined in Ebrahim et al. (2024a). Table 1 summarizes
115 several review studies that have explored landslide prediction approaches, many of which focus
116 on a single methodology. Notably, scientometric analysis has been infrequently applied in this
117 context. The novelty of this study lies in several key contributions: it presents a combined
118 scientometric and systematic review, utilizing bibliometric analysis to compare the accuracy of
119 different models; offers a comprehensive explanation of the initial conditions and theoretical
120 geotechnical and hydrological concepts underlying rainfall-induced landslides; and includes
121 both empirical statistical thresholds and physically based causative models, along with



122 deterministic physical models and landslide susceptibility maps in Parts I and II. Furthermore,
 123 this study highlights the latest advancements in the field.

124 This two-part review explores the evolution of different approaches, starting with a
 125 macroscopic perspective based on input parameters and initial conditions, followed by a
 126 microscopic examination of alternative analysis models for the same method. The structure of
 127 this research is as follows: Section 2 outlines the research methodology; Section 3 highlights
 128 the scientometric analysis; Section 4 focuses on the systematic analysis, which is divided into
 129 two subsections: 1) empirical-statistical thresholds, and 2) physically based causative
 130 thresholds; Section 5 provides the discussion; Section 6 presents the conclusion and future
 131 work; Section 7 summarizes the notations and abbreviations; and Section 8 lists the references.

132 **Table 1.** Available review articles for landslide prediction techniques.

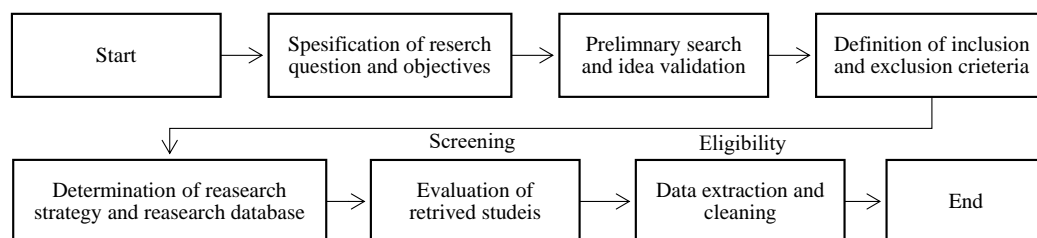
Study	Content
Zhang et al. (2011)*	Geotechnical and hydrological concepts related to rainfall-triggered landslides
Chae et al. (2017)*	Landslide susceptibility, modeling of runout, monitoring, and early warning systems
Segoni et al. (2018)*	Rainfall-based landslide thresholds
Merghadi et al. (2020)*	Application of machine learning algorithms for assessing landslide susceptibility
Shano et al. (2020)*	Overview of various prediction methods, emphasizing statistical models
Yanbin et al. (2022)*	Use of machine learning techniques in landslide susceptibility analysis
Zou & Zheng (2022)**	Scientometric review, limited physical prediction models, and case studies
Huang et al. (2022)***	Landslide susceptibility models based on Geographic Information System (GIS) data
Petrucci (2022)*	Analysis of the main causes behind landslide-related fatalities
Vung et al. (2023)*	Exploration of challenges, opportunities, and future research directions for rainfall-induced landslides
Ebrahim et al. (2024a)*	Deterministic and susceptibility-based landslide prediction models
Ebrahim et al. (2024b)*	Time series-based prediction models for landslides
*Refers to systematic reviews; **Scientometric analysis; ***Bibliometric approach	

133 **METHODOLOGY OF THE STUDY.**

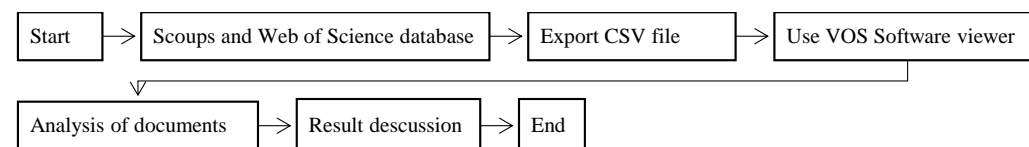
134 This study employs a mixed review approach, combining both quantitative (scientometric) and
 135 qualitative (systematic) methods. The aforementioned technique is offered to assist researchers



136 in improving systematic review reporting using scientometric analysis. In addition, it sheds
 137 light on the difficulty of performing manual searches on database engines. This approach
 138 integrates the strengths of both strategies, which have been widely used in other fields (Yin et
 139 al., 2019; Wuni & Shen, 2020; Ebrahim et al., 2024c). As a result, a mixed review strategy was
 140 used to meet the study's primary objective in the field of landslide prediction. Figure 3
 141 illustrates the methodical flow for a systematic review, which consists primarily of three
 142 processes: identification, screening, and eligibility. Regarding scientometric analysis, Figure 4
 143 demonstrates the steps of the aforementioned analysis, which mainly consist of gathering
 144 bibliometric data, exporting bibliometric data to an appropriate program, evaluating data, and
 145 discussing results.



147 **Figure 3.** Methodological flow for a systematic review



149 **Figure 4.** Methodological flow for scientometric analysis.

150 **Identification Process.**

151 Landslides can be classified based on various factors, such as geology, engineering,
 152 environmental science, ecology, meteorology, atmospheric science, geochemistry, geophysics,
 153 physical science, and water resources (Zou & Zheng, 2022). Additionally, as highlighted in the



154 keyword mapping by Zou and Zheng and Ebrahim et al. (Zou & Zheng, 2022; Ebrahim et al.,
155 2024c), landslides are associated with a wide range of keywords. Therefore, the research
156 process begins with the identification of relevant studies on landslides, guided by the authors'
157 perspectives. This section outlines the use of keywords, search databases, and inclusion and
158 exclusion criteria to filter the collected papers. A standard review methodology for screening
159 the selected studies is detailed in Section 5.

160 **Database and Keyword Selection**

161 To ensure a comprehensive retrieval of relevant articles, it is recommended to use multiple
162 databases in a systematic review. The three most commonly utilized databases in engineering
163 research are Scopus, Web of Science, and Google Scholar. Scopus and Web of Science are also
164 compatible with advanced scientific mapping tools like VOS Viewer. This study focuses
165 primarily on Scopus and Web of Science as the main sources for searching landslide prediction
166 literature. Additionally, Google Scholar is employed in the snowballing strategy. Once the
167 search databases are selected, key terms such as "landslide prediction" are identified to cover
168 all available datasets and prediction techniques.

169 **Criteria for Inclusion and Exclusion.**

170 In any systematic review, inclusion and exclusion criteria play a vital role in filtering search
171 results and prioritizing the most relevant studies to the research question. This study applied
172 the following inclusion criteria: 1) studies focused on landslide prediction, aligned with the aim
173 outlined in the INTRODUCTION section; 2) studies published up to 2024; 3) articles published
174 in peer-reviewed journals; 4) studies published as research articles or review papers; and 5)
175 studies published as final versions. The exclusion criteria were: 1) papers published in
176 languages other than English; 2) studies lacking available full text; 3) manuscripts from subject
177 areas outside of engineering; and 4) articles published in non-journal sources. The search
178 strategy in Scopus and Web of Science with inclusion and exclusion criteria was as follows:



179 Scopus: TITLE-ABS-KEY("landslide prediction") AND PUBYEAR > 1999 AND PUBYEAR
180 < 2025 AND (LIMIT-TO(SUBJAREA, "ENGI")) AND (LIMIT-TO(DOCTYPE, "ar") OR
181 LIMIT-TO(DOCTYPE, "re")) AND (LIMIT-TO(PUBSTAGE, "final")) AND (LIMIT-
182 TO(LANGUAGE, "English")).

183 Web of Science: [https://www.webofscience.com/wos/woscc/summary/94fee090-b6a4-4ecf-](https://www.webofscience.com/wos/woscc/summary/94fee090-b6a4-4ecf-a951-5b904e6fb3a8-01155ef62f/recently-added/1)
184 [a951-5b904e6fb3a8-01155ef62f/recently-added/1](https://www.webofscience.com/wos/woscc/summary/94fee090-b6a4-4ecf-a951-5b904e6fb3a8-01155ef62f/recently-added/1)

185 **Screening and Assessment of Collected Articles.**

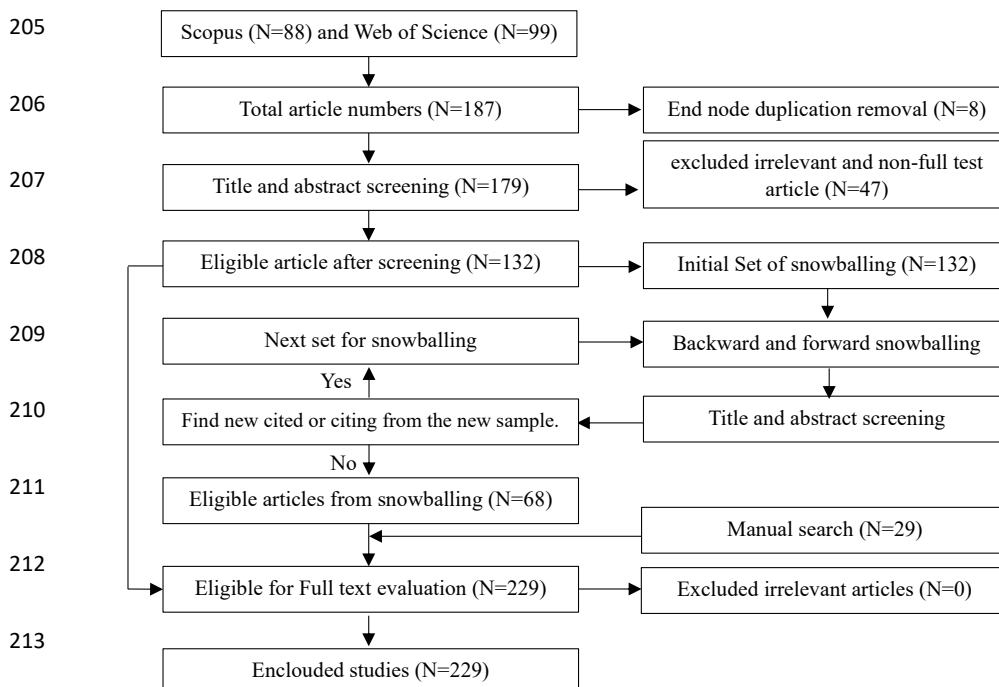
186 The Scopus and Web of Science databases provided 88 and 99 articles, respectively. Initially,
187 8 duplicate articles were removed. The low number of duplicates can be attributed to the
188 differing criteria between the Web of Science and Scopus databases, as well as the broad range
189 of related keywords. The systematic review and meta-analysis (PRISMA) procedure (Moher
190 et al., 2009) was then applied to evaluate and assess the collected articles (see Figure 5). As a
191 result, 47 papers were excluded due to irrelevance or unavailability of the full text. After
192 evaluating the full texts of the remaining articles, 132 articles met the inclusion criteria.

193 The backward and forward snowballing approach was then employed to identify
194 additional studies that were not retrieved through the Scopus and Web of Science searches
195 (Wohlin, 2014). The 132 included papers were used as the starting point for the backward and
196 forward snowballing search strategy's pertinent investigations. Unlike "forward snowballing,"
197 which involves locating new publications based on those that cite the paper under investigation,
198 "backward snowballing" involves searching the reference lists of each paper in the start set for
199 pertinent papers. The new set is made up of the newly discovered articles from this procedure.
200 The cycle was repeated until no further documents were discovered. Sixty-eight relevant new
201 articles were discovered because of this search approach. It should be noted that 29 papers were
202 included during the manual search for articles that were conducted during the full-text review,



203 making a total of 229 articles acceptable for inclusion. The whole screening and evaluation

204 process are summarised in Figure 5.



214 **Figure 5.** Screening and selecting flow diagram: PRISMA.

215 In this section, we listed the number of papers included in the study as part of the

216 methodological process, specifically, the selection criteria and scope of the literature review.

217 This is intended to provide context for the analysis that follows. It should be emphasized that

218 the number of manuscripts illustrated above in Figure 5 are reviewed in two parts: this study

219 (part i) and the study of Ebrahim et al. (2024a) which has been published. The actual analysis

220 and interpretation of the selected papers begin in the SCIENTOMETRIC ANALYSIS Section.

221 SCIENTOMETRIC ANALYSIS

222 In this section, we provide a detailed analysis of the selected studies. The scientometric analysis

223 commenced after completing the screening process to examine the relationships among

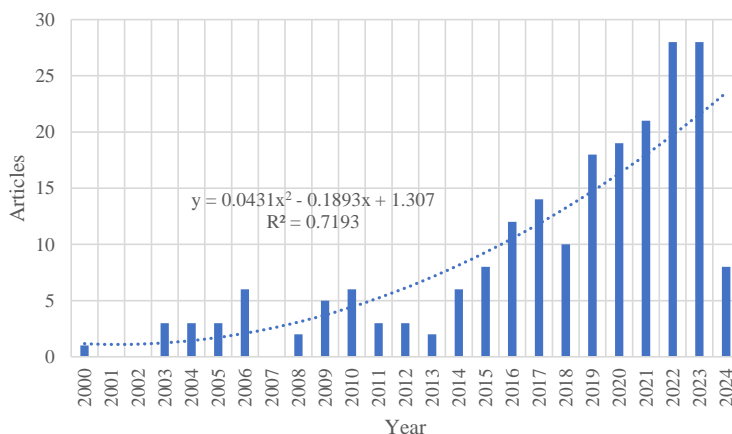
224 authors, keywords, publications, and countries within specific research areas. This analysis was



225 conducted using the open-source VOSviewer software tool (van Eck & Waltman, 2010), a
226 widely recognized visualization tool employed in this study to analyze the results. The primary
227 goal of the scientometric analysis is to ensure that the findings are meaningful and relevant for
228 inclusion in the systematic review. A total of 229 manuscripts, identified through snowballing
229 and manual searches, were analyzed using VOSviewer software.

230 **The Trend In Annual Publications For Landslide Prediction.**

231 Figure 6 illustrates the annual publication trend of landslide prediction-related studies. From
232 2000 to 2014, the average number of articles published per year was approximately three. The
233 publishing rate thereafter experienced a significant jump from 8 to 28 publications between
234 2015 and 2023 in which the researcher's primary area of interest is landslide prediction for the
235 past nine years. This trend is not unexpected, considering the increasing global focus on
236 reducing the loss of human life, property, and economic assets due to landslides. Then, it
237 becomes apparent that the previously indicated rate abruptly dropped to only 8 manuscripts in
238 2024. The decline is because this study (part ii) was completed in May 2023 (Ebrahim et al.,
239 2024a) while part i was before the mid-end of 2024 as more research is expected to be
240 published.



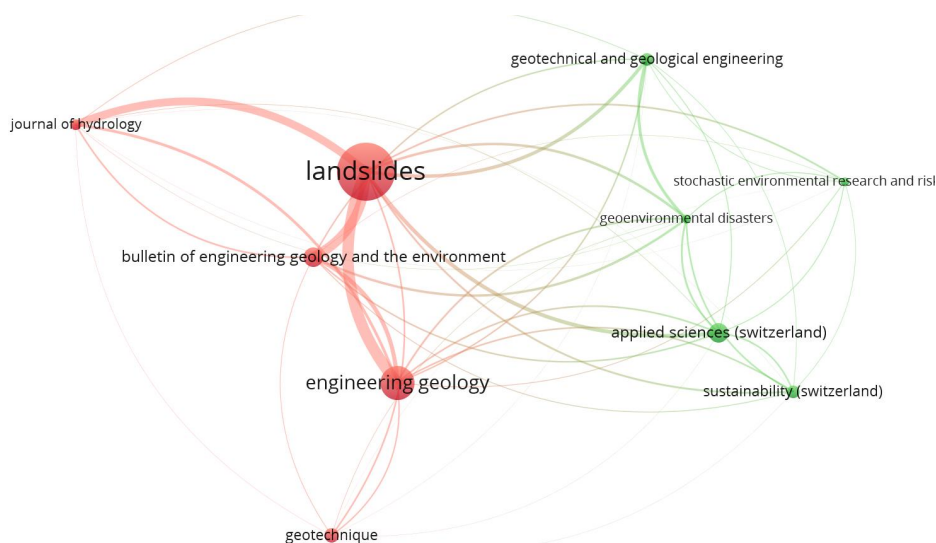
241

242 **Figure 6.** The total number of articles per year related to landslide prediction.



243 **Leading Journals in Landslide Prediction Contributions**

244 The VOSviewer software has been used to identify the leading journals in landslide prediction,
245 as shown in Table 2. This analysis helps guide researchers in selecting reputable journals in
246 this field. Two thresholds were applied during the VOSviewer analysis: 1) a minimum of five
247 papers per journal, and 2) a minimum of ten citations per journal. The unit of analysis was
248 "sources," and the analysis type employed was "bibliographic coupling." As a result, 10
249 journals out of 86 met these criteria (Figure 7). It's important to note that there are no
250 universally established thresholds for the number of manuscripts or citations per journal (Zou
251 & Zheng, 2022). Node size in Figure 7 highlights the journals' influence as weighted by
252 publications. The number of linkages between a journal and other journals is represented by its
253 total link strength (van Eck & Waltman, 2009). Table 2 presents the 10 journals where the
254 highest publishing and topmost cited journal is "Landslides", with 32 articles and 4195
255 citations.



256 **Figure 7.** The top journals contributing to the field of landslide prediction.
257

258 **Table 2.** The top journals contributing to landslide prediction research.



No	Source	Documents	Citations	Total strength link
1	Landslides	32	4195	1190
2	Engineering Geology	19	1414	733
3	Bulletin of Engineering Geology and the Environment	11	317	625
4	Applied Sciences (Switzerland)	11	178	354
5	Géotechnique	8	6117	142
6	Geotechnical and Geological engineering	7	173	330
7	Sustainability (Switzerland)	7	76	253
8	Journal of Hydrology	6	1456	396
9	Geoenvironmental disaster	5	404	405
10	stochastic environmental research and risk assessment	5	290	172

259

260 **Active Nations in Landslide Prediction.**

261 The identification of top scientists, laboratories, organizations, authors, and nations is made
262 easier with an understanding of the scientific collaboration network in any subject of study.

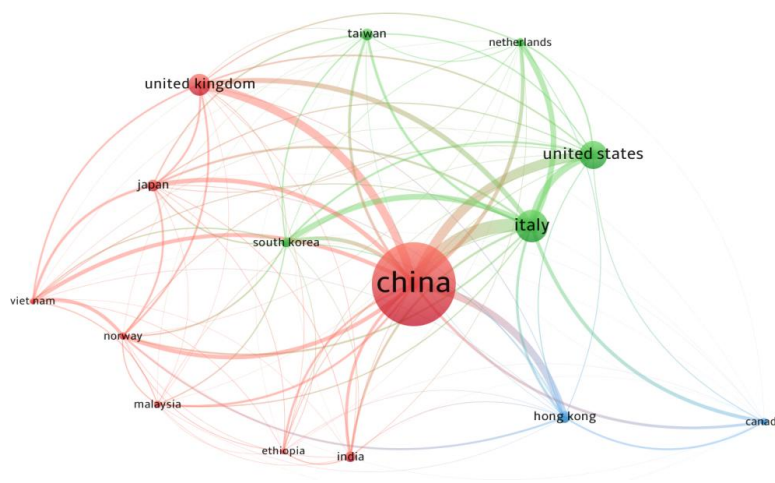
263 This can greatly facilitate academic collaboration. The thresholds mentioned above were
264 applied, with "countries" as the unit of analysis and "bibliographic coupling" as the analysis
265 type. Out of a total of 44 countries, only 15 met the criteria. The size of the node in Figure 8

266 represents the influence of each country in the field, weighted by the number of publications.

267 To give two examples, China and Italy have the most publications worldwide, recording 77 and
268 31 articles, respectively. Ethiopia has 5 publications and poor connections to other nations.

269 Additionally, Table 3 presents information on the top five countries contributing to landslide
270 prediction research. Moreover, both academic and industrial practitioners seeking innovative
271 solutions for landslides can benefit from understanding the collaborative network of countries

272 that are investing more in this field.



273
 274 **Figure 8.** Top countries publishing in landslide prediction.

275 **Table 3.** Top five prominent and publishing countries relevant to landslide prediction.

Country	Documents	Citations	Total link strength
China	77	3896	7348
Italy	30	5007	5622
United States	26	5146	2963
United Kingdom	20	6299	2623
Japan	11	2351	2098

276
 277 **Article Co-Citation Analysis in Landslide Prediction.**

278 The total number of citations for any publication indicates its contribution to the field. Thus,
 279 this section includes citations of the most cited publications in landslide prediction research.
 280 Since there is no strong correlation between these publications, the top 10 cited articles were
 281 selected directly from the Scopus and Web of Science databases. These articles span from 2000
 282 to 2024. To mitigate the issue of older research receiving more citations than more recent work,
 283 a normalized citation measure was employed in this study. The citation count for each article
 284 was normalized by dividing the number of citations by the average number of citations for all
 285 articles published in that year (van Eck & Waltman, 2009). Consequently, the top five papers



286 based on normalized citation (NS) are: (Merghadi et al., 2020; Soga et al., 2016; Froude &
 287 Petley, 2018; Ebrahim et al., 2024c; Hungr et al., 2014), as presented in Table 5.

288 **Table 5.** Top 10 cited articles according to normalized citations (NS).

Author	Article	Journal	Citation	NS
Merghadi et al. (2020)	Machine learning methods for landslide susceptibility studies: A comparative overview of algorithm performance	Earth-Science Reviews	603	8.20
Soga et al. (2016)	Trends in large-deformation analysis of landslide mass movements with particular emphasis on the material point method	Géotechnique	383	5.80
Froude & Petley (2018)	Global fatal landslide occurrence from 2004 to 2016	Natural Hazards and Earth System Sciences	1164	5.62
Ebrahim et al. (2024c)	Recent Phenomenal and Investigational Subsurface Landslide Monitoring Techniques: A Mixed Review	Remote Sensing	7	4.90
Hungr et al. (2014)	The Varnes classification of landslide types, an update	Landslides	2274	4.32
Ikram et al. (2023)	A novel swarm intelligence: cuckoo optimization algorithm (COA) and SailFish optimizer (SFO) in landslide susceptibility assessment	Stochastic Environmental Research and Risk Assessment	37	4.16
Zhang et al. (2021a)	Application of an enhanced BP neural network model with water cycle algorithm on landslide prediction	Stochastic Environmental Research and Risk Assessment	140	3.50
Mondini et al. (2023)	Deep learning forecast of rainfall-induced shallow landslides	Nature communications	31	3.49
Chae et al. (2017)	Landslide prediction, monitoring and early warning: a concise review of state-of-the-art	Geosciences Journal	267	3.03
Long et al. (2022)	A multi-feature fusion transfer learning method for displacement prediction of rainfall reservoir-induced landslide with step-like deformation characteristics	Engineering Geology	47	2.94

289

290 **Keyword Co-occurrence Mapping in Landslide Prediction.**

291 The VOSviewer software is capable of identifying the most frequently used keywords by
 292 selecting "co-occurrence" as the analysis type and "all keywords" as the unit of analysis. For
 293 this study, the minimum number of occurrences for a keyword was set to ten. As a result, only
 294 45 keywords out of 1785 met this criterion, as shown in Figure 9. The size of each keyword
 295 node is proportional to its frequency of occurrence. Notably, the most commonly used
 296 keywords, "landslide" and "landslides," have the largest node size. The analysis reveals three
 297 distinct clusters: the blue cluster, which is associated with landslide susceptibility maps; the
 298 red cluster, which focuses on physical models; and the green cluster, which pertains to



314 landslide. For the local scale, empirical-statistical thresholds, triggering-physical thresholds,
315 and physical-deterministic models can be adapted based on the available data and the required
316 accuracy of the prediction. However, landslide susceptibility, landslide risk, and landslide
317 vulnerability maps can be utilized on a national scale. Figure 11 summarises the whole process
318 adopted in this review based on the aforementioned classification. This Figure will be discussed
319 in detail in two parts of this study: part i (this manuscript) and part ii (Ebrahim et al., 2024a)
320 which has been published.

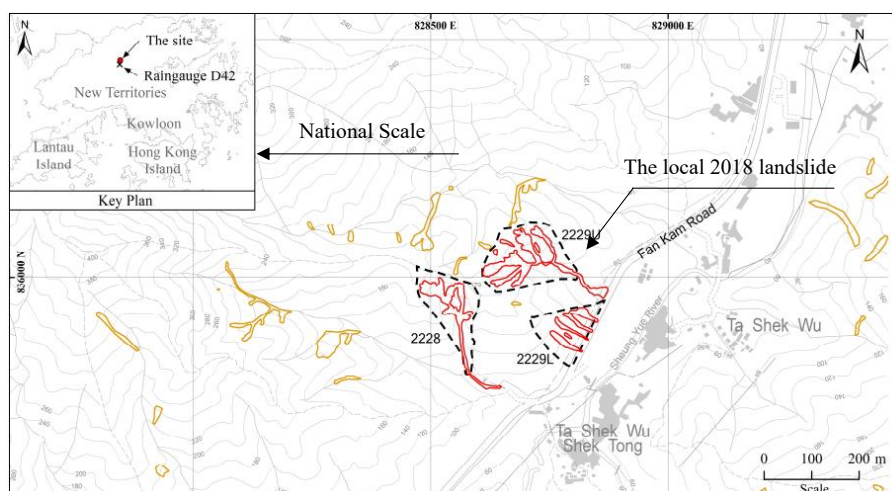
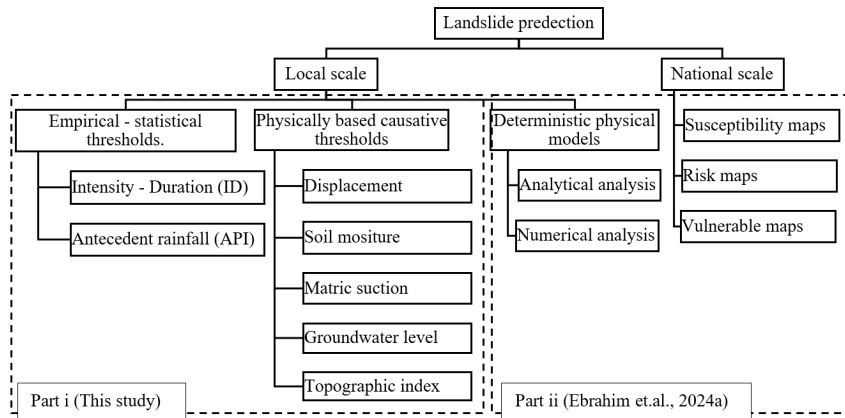


Figure 10. The 29th August 2018 landslides, above Fan Kam Road, Pat Heung, Hong Kong (AECOM, 2019) (By courtesy of Geotechnical Engineering Office HKSAR; used with permission)



321

322 **Figure 11.** Classifications of landslide prediction models. Part ii has been already published
 323 (Ebrahim et al., 2024a).

324 In this section, we present a comparative analysis based on a comprehensive review of
 325 the literature. All figures and comparisons are created by the authors to synthesize and highlight
 326 key trends and findings across multiple studies. While the original data and results are from
 327 previously published research, each study is cited in the text. Given the large number of studies
 328 compared in some of the plots, it is impractical to list all sources directly below each figure.
 329 Instead, readers are referred to the relevant citations in the text for detailed references to the
 330 original studies.

331 **Empirical-Statistical I-D Thresholds.**

332 *Intensity-Duration Thresholds.*

333 Understanding the factors that trigger landslides is essential. Researchers have started
 334 predicting landslide occurrences using simple empirical thresholds (Caine, 1980; Hong et al.,
 335 2006; Lee et al., 2014; Gariano et al., 2019). Historically, landslides have been linked to
 336 rainfall, with landslides often depending on rainfall conditions. By analyzing historical data on
 337 rainfall intensity (I) and duration (D) for specific regions, rainfall thresholds can be established



338 as a minimum limit beyond which landslides may occur (Wu et al., 2015; Zhao et al., 2019a).
339 As Guzzetti et al. (2024) put it, “Rainfall thresholds are defined by a minimum amount of
340 rainfall that, when exceeded, can trigger landslides. These thresholds are crucial for predicting
341 potential landslides and form a core component of many landslide early warning systems.
342 Using statistical regression, Equation 1 proposed by (Caine, 1980) as well as Equation 2
343 presented by (Hong et al., 2006) are examples of these thresholds. These equations apply only
344 to a certain scenario. Furthermore, the general equation is presented by Equation 3 proposed
345 by (Peruccacci et al., 2017). Equation 3 was developed for an area that suffers from landslides
346 using a new technique called CTRL-T (Gariano et al., 2019). CTRL-T is a recent model that
347 can automatically extract rainfall (Melillo et al., 2018).

$$1) I = 14.82D^{-0.39} \qquad 2) I = 15.58D^{-0.52} \qquad 3) E = (\epsilon \pm \Delta\epsilon)D^{(\zeta \pm \Delta\zeta)}$$

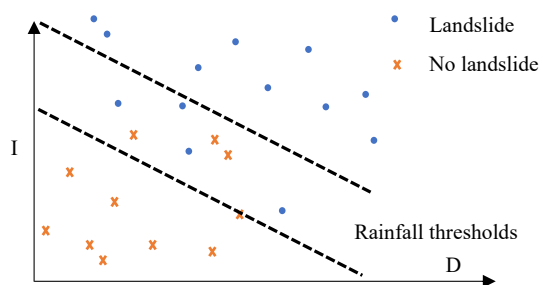
348 Where E represents the rainfall event, ϵ is the scaling parameter, and ζ is the shape
349 parameter, which defines the intercept and slope of the power law curve, respectively.
350 Additionally, $\Delta\epsilon$ and $\Delta\zeta$ denote the uncertainties associated with these two parameters

351 Furthermore, Ering and Babu (2020) developed Intensity-Duration (I-D) thresholds
352 through the Forecasting of Landslides Induced by Rainfall (FLaIR) model. FLAIR can deal
353 with varied rainfall inputs using the gamma-type transfer function $\Xi(t)$ (Equation 4). Figure 12
354 illustrates that while these thresholds may offer high accuracy, the occurrence of false positive
355 alarms limits their predictive effectiveness (Hong et al., 2018; Zhao et al., 2019a; Uwihirwe et
356 al., 2020). To clarify, the intensity-duration (I-D) concept involves determining a critical
357 intensity threshold, which, when exceeded, triggers landslides. These critical intensity values
358 are fixed for a specific duration.

$$359 \quad 4) \Xi(t) = t^{\nu-1} \exp\left(-\frac{t}{T}\right) / T^{\nu} \Gamma(\nu),$$



360 where v denotes the dimensionless parameter, and T denotes the temporal scale.



361

362 **Figure 12.** Uncertainties of rainfall thresholds.

363 *Antecedent Rainfall Thresholds.*

364 To address the limitations of I-D thresholds, causal thresholds have been proposed. Rainfall
365 influences several interconnected factors, such as increasing ground saturation, soil weight,
366 groundwater levels, soil erosion, and the effective stress of the soil, which in turn reduces the
367 safety factor for slope stability (Chhorn et al., 2016). When analyzing rainfall-induced
368 landslides, it is important to consider the significant role of antecedent rainfall, as it can also
369 have a substantial impact on landslide occurrence (Hong et al., 2018). This factor helps account
370 for other causative elements that contribute to landslide events (Lee et al., 2014; Chhorn et al.,
371 2016; Hong et al., 2018; Uwihirwe et al., 2020). This can be illustrated by the infiltration,
372 storage, and evaporation process, which mainly relies on the timing of the porewater pressure
373 change in the subsurface soils (Uwihirwe et al., 2020). However, the specific duration of
374 antecedent rainfall that is most critical for landslide prediction remains unknown (Chhorn et
375 al., 2016). Lee et al. (2014) proposed the antecedent precipitation index (API), as shown in
376 Equations 5, 6, and 7. Meanwhile, Huang et al. (2015) incorporated both the maximum hourly
377 rainfall intensity along with the accumulated current rainfall, as well as the rainfall from the
378 past six days.



$$5) \text{ API}_{30} = 115 + 1.2 \times 10^{-12} N^{10.6} \quad 6) E_3 = -0.726 \text{ API}_{30} + 295.0 \quad 7) E_3 = -0.726 \text{ API}_{30} + 194.3$$

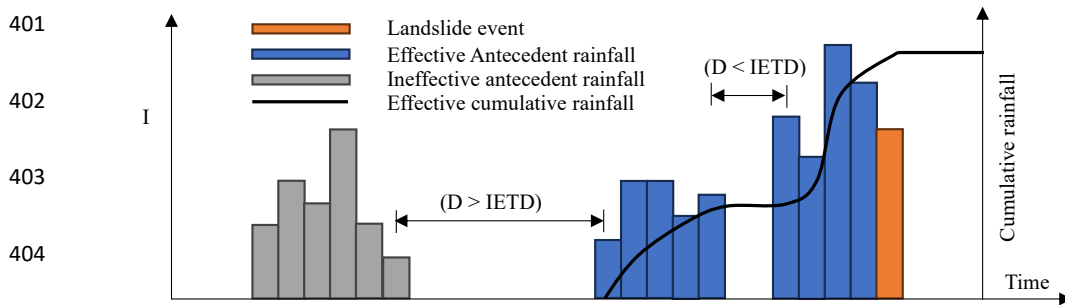
379 Where API_{30} is the 30-day antecedent precipitation index, N is the number of rainy days
380 within the 30 days concerned, and E_3 is the commutative 3-day rainfall. Equation 6 is for a
381 major landslide, and Equation 7 is for a medium landslide.

382 Hong et al. (2018) applied inter-event time definitions (IETDs) and found that the highest
383 accuracy was achieved with an IETD of 12 hours. IETD can be defined as the interval of time
384 between two distinct rainfall occurrences. IETDs offer a viable way of analyzing antecedent
385 rainfall, as shown in Figure 13. Chhorn et al. (2016) proposed various durations rather than a
386 single crucial time to increase forecast accuracy. The best combination that gave a probability
387 of 58.5% was found to be antecedent 1 hour, 15 hours, and 19 days. Uwihirwe et al. (2020)
388 used the Bayesian probabilistic approach, maximum true skill statistic, and minimum radial
389 distance to determine that rainfall on the occurrence day, along with antecedent rainfall from
390 the previous 10 days, provided the best accuracy, achieving an AUC of 0.669 (see Figure 14-
391 a). Unlike previous studies, Zhao et al. (2019b) developed a modified API to consider the
392 variation in the evaporation process and the maximum soil moisture capacity. The modified
393 API threshold surpasses the general form of I-D thresholds adopted by (Brunetti et al., 2010)
394 (Figure 14-b). Aryastana et al. (2024) concluded that considering a cumulative rainfall of 30
395 days (i.e., antecedent effect) could improve the accuracy of the traditional thresholds achieving
396 an accuracy of over 90%. Ebrahim and Zayed (2024) found that considering Hong Kong as a
397 case study, the recovery time can vary between two weeks to approximately five weeks.

398

399

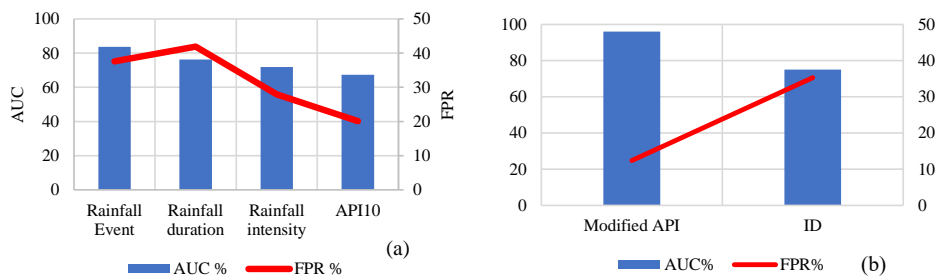
400



405 **Figure 13.** Rainfall pattern with effective cumulative rainfall for different non-rainfall periods
 406 (D).

407 *I-D Thresholds Prediction Accuracy.*

408 The accuracy of any model depends on several factors, including the availability of data,
 409 rainfall parameters, and the specific characteristics of each case study. In a recent study,
 410 Uwihirwe et al. (2020) utilized the Bayesian probabilistic approach, maximum true skill
 411 statistic, and minimum radial distance to assess the accuracy of various rainfall-triggering
 412 thresholds. As presented in Figure 14-a, the best accuracy (AUC) is achieved using rainfall
 413 events. On the other hand, this method suffers from a high false positive rate (FPR). In contrast,
 414 adopting simple causative antecedent rainfall (API₁₀) reduced the FPR. Similarly, Zhao et al.
 415 (2019b) proved that the modified API can achieve better results than I-D models (see Figure
 416 14-b).



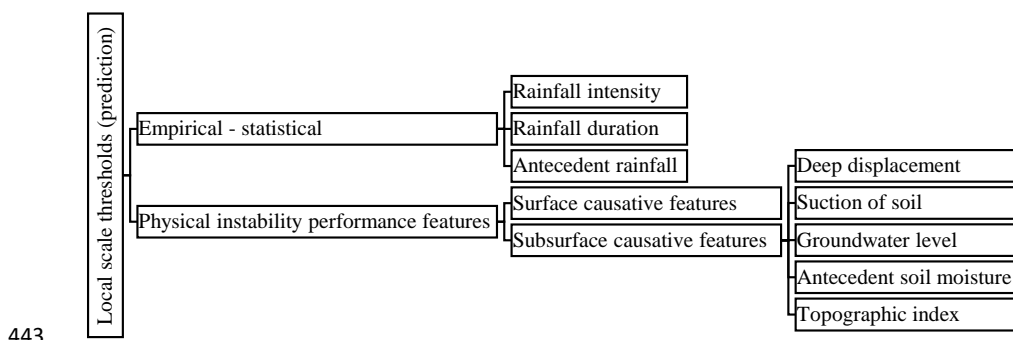
417 **Figure 14.** Accuracy (AUC) and true false positive rate (FPR) for different rainfall variables.



418 As illustrated above, considering the slope response in terms of antecedent effect (i.e.,
419 moisture dynamics) helped the model to achieve better accuracy than relying only on rainfall.
420 These trigger thresholds for landslide causation have been recently proposed by several studies
421 (Lee et al., 2014; Huang et al., 2015; Chhorn et al., 2016; Bogaard & Greco, 2018; Hong et al.,
422 2018). These methods are simple and consider only antecedent rainfall as a causative trigger
423 of landslides. Therefore, different causative features are required for further improving the
424 prediction accuracy and will be discussed in section (5.2) “Physically Based Causative
425 Thresholds”.

426 **Physically Based Causative Thresholds and Prediction.**

427 If a landslide occurs during a rainfall period where the total precipitation reaches its peak, this
428 period is considered the critical duration. However, if the landslide happened while the
429 cumulative antecedent rainfall was not at its highest, then the landslide was caused by factors
430 other than rainfall (Chhorn et al., 2016). The connection between rainfall-induced landslides
431 and the reduction in soil strength is affected by several factors, such as slope infiltration,
432 vegetation cover, topography, and hydraulic properties. The amount of rainfall cannot solely
433 determine the occurrence of landslides, as other factors may influence their likelihood.
434 Therefore, relying solely on a rainfall threshold is insufficient in explaining the occurrence of
435 landslides. Furthermore, once established, the threshold is the same regardless of the soil
436 conditions (Hong et al., 2018; Zhao et al., 2019a). Integrating rainfall as an external trigger
437 with the causative factors of landslides provides reasonable accuracy with a low false positive
438 rate. These causative features (i.e., instability indicators) can be as follows: antecedent rainfall
439 (discussed earlier) (Hong et al., 2018); moisture content (De Luca & Versace, 2017; Bezak et
440 al., 2019; Zhao et al., 2019b); topographic thresholds (Ho et al., 2012); displacement
441 (Bednarczyk, 2018); suction of the soil (Davar et al., 2022); and groundwater level (Cao et al.,
442 2020). Therefore, this section is arranged as shown in Figure 15 to list such applications.



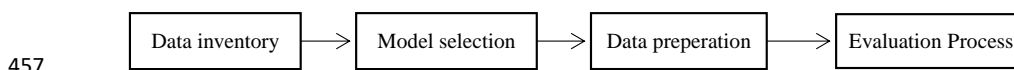
443

444 **Figure 15.** A schematic view for regional thresholds (prediction).

445 It should be emphasized that the term physically-based causative refers to an approach
 446 that combines rainfall, as the main triggering factor, with additional indicators of instability to
 447 enhance model accuracy. While rainfall remains a critical trigger, other factors—such as
 448 moisture content, topographic thresholds, displacement, soil suction, and groundwater level—
 449 are integrated to improve the robustness of landslide predictions. In this section, we examine
 450 these secondary indicators of instability, emphasizing how they complement primary causative
 451 factors such as rainfall, thereby offering a more holistic understanding of landslide dynamics.

452 *Displacement Instability Performance and Prediction.*

453 Landslide displacement prediction can be categorized into four key processes: data inventory
 454 and input parameters, model selection, data preparation (including sampling and
 455 decomposition), and model evaluation, as presented in Figure 16. Each process will be
 456 discussed in detail as follows.



457

458 **Figure 16.** Landslide displacement prediction process.

459 1. Data inventory and input model parameters.

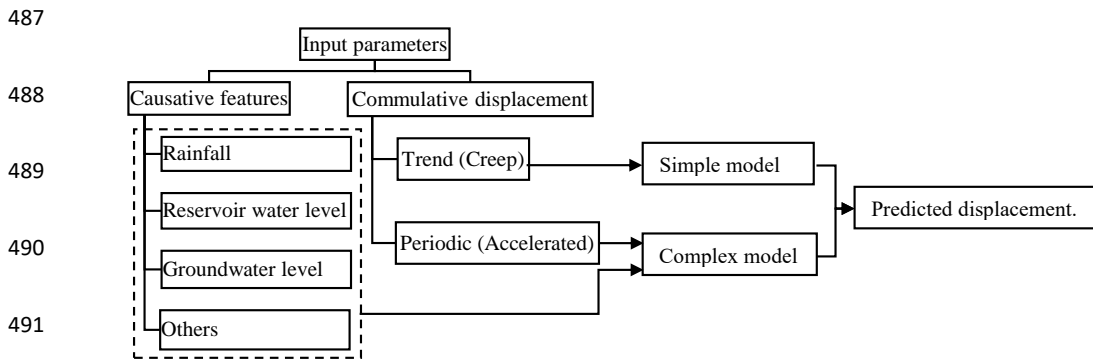
460 When enough monitoring data are collected, numerous mathematical approaches can be
 461 utilized to predict landslides with reasonable accuracy. Full-site investigations, real-time



462 monitoring, and laboratory tests can be used as quick warning signs. For example, the
463 occurrence of significant pore-pressure variations could serve as an early warning indicator
464 before substantial movements take place. However, this mainly depends on the precision of the
465 geotechnical data interpretation and the selection of monitoring locations. Since the
466 geotechnical and hydrological properties require massive work to provide accurate datasets and
467 have a limited generalization ability (Niu et al., 2021), the monitoring of landslide movements
468 offers a viable way to overcome the aforementioned drawbacks (Lian et al., 2014). Various
469 researchers have based their studies on continuously monitored displacement data using GPS
470 data (Lian et al., 2014; Yao et al., 2015; Li et al., 2021; Niu et al., 2021; Zhang et al., 2021a;
471 Zhang et al., 2021b; Wang et al., 2023b), GNSS (Krkač et al., 2017), optical fiber (Han et al.,
472 2021), and fiber Bragg grating technology (Shentu et al., 2022). One of the most studied areas
473 is the Three Gorges region near the Yangtze River in China, which experiences landslides due
474 to rainfall and fluctuations in reservoir levels (Lian et al., 2014; Yao et al., 2015; Cao et al.,
475 2016; Lian et al., 2016; Liu et al., 2016; Xing et al., 2019; Gao et al., 2020; Han et al., 2021;
476 Li et al., 2021; Zhang et al., 2021a; Zhang et al., 2021b; Long et al., 2022; Wang & Zhao, 2023;
477 Wang et al., 2023a; Wang et al., 2023b). In addition to historical displacement data, the model
478 inputs also include other causative factors as outlined in Table 6. These factors are as follows:
479 rainfall data factor that can reach up to 75 features (Krkač et al., 2017); antecedent and rolling
480 rainfall, rainfall intensity, and effective rainfall (Liu et al., 2016); groundwater level that can
481 count 10 variables (Krkač et al., 2017); climate features (Krkač et al., 2020); reservoir water
482 level parameters (current value, antecedent change rate, average value, etc.) (Zhang et al.,
483 2021a; Wang et al., 2023b); and porewater pressure (Sasahara, 2017; Bednarczyk, 2018). A
484 schematic view can summarize the aforementioned variables presented in Figure 17.

485

486



492 **Figure 17.** Schematic view of the input parameters.

493 2. Model selection.

494 First, researchers have adopted regression analysis due to its advantages, including the fact that
495 it does not require prior information to create the function, is simple to understand, and can
496 estimate the contributions of the input variables (Zhang et al., 2016). Bednarczyk (2018)
497 correlated the relationship between the magnitude of displacement (S) with cumulative rainfall
498 (R) and cumulative pore pressure difference using linear regression. However, geotechnical
499 monitoring data (i.e., pore pressure) are lacking. Similarly, Chen et al. (2018) used linear
500 correlation to examine the relationship between rainfall, reservoir level fluctuations, and
501 surface displacement. On the other hand, the relation between the aforementioned variables is
502 complex and needs to be investigated with nonlinear relationships. The reason for such
503 complex behavior is the time lag between the peak external triggering and peak displacement
504 of the slope. This lag is variant, with the case study ranging from approximately 6 months to 6
505 days (Chen et al., 2018) (Figure 18). Abolmasov et al. (2015) tried to correlate the displacement
506 with the river level, which exhibited a low correlation ($R^2 = 0.145$) considering the time lag
507 effect and the accelerated displacement concept (refer to Figure 19), Sasahara (2017) concluded
508 that regression analysis using hyperbolic relationships provides reasonable prediction accuracy
509 for temporal variation of the shear strain and surface displacement using pore water pressure
510 and groundwater level, respectively. However, this study was based on a laboratory physical



511 uniform soil model. However, Natural slopes are made up of more complicated, non-uniform
 512 soil layers. Li et al. (2021) adopted a new mathematical short-term forecasting of landslides
 513 (STFL) to predict the failure time. This method achieved accurate prediction ($R^2 > 0.99$) (refer
 514 to Equation 8 and Figure 19). In the tertiary stage, when the tangential angle exceeds 79° , the
 515 displacement parameters can be employed to obtain the equation unknowns using the
 516 Levenberg–Marquardt (LM) algorithm.

517 8) $S = P_1(P_2^{P_3 t} - 1) / (P_0 - t)$, where $P_0, P_1, P_2,$ and P_3 are the simulated parameters, t denotes time,
 518 and S denotes displacement.

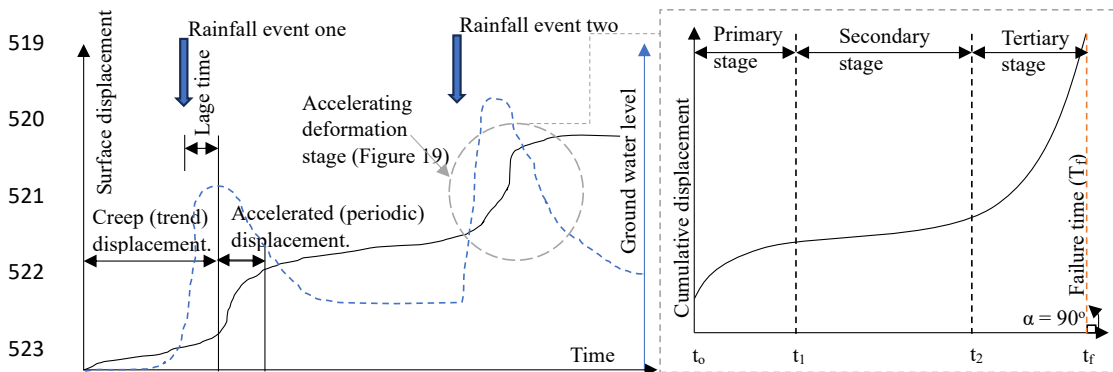


Figure 18. The relationship among rainfall events, **Figure 19.** Accelerated surface displacement, and groundwater level with time. deformation stage.

524 The thresholds for landslide deformation vary from one landslide to another.
 525 Displacement thresholds are thus not recommended. Shentu et al. (2022) proposed alert limits
 526 based on the direction angle of the displacement rather than its value. However, the tangential
 527 angle of the curve changes when the scales of either the displacement or time coordinates are
 528 adjusted. Consequently, Li et al. (2021) suggest using the displacement rate. However,
 529 researchers have tried to predict the displacement before the real failure time for early warning
 530 purposes and to create a displacement threshold.



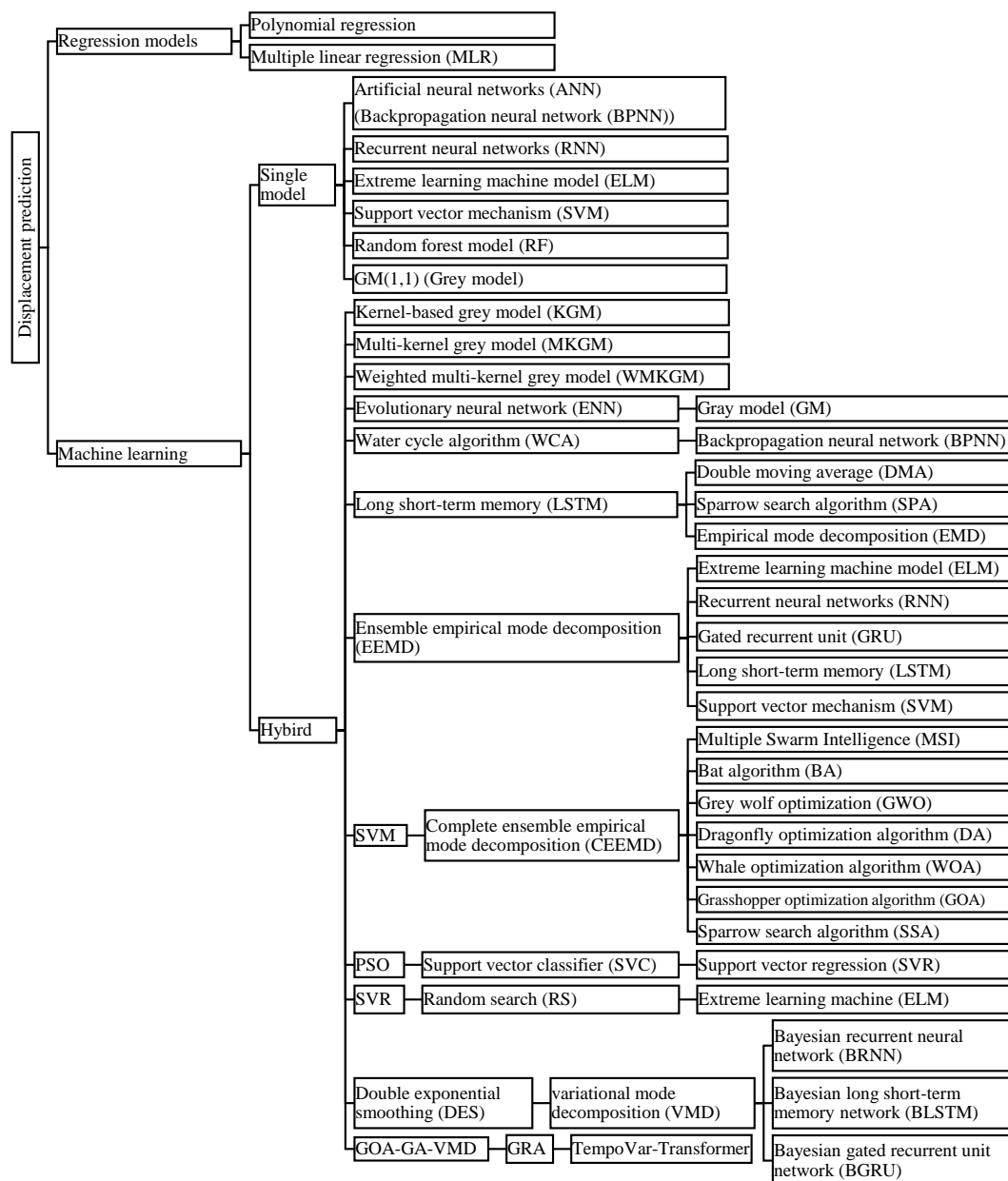
531 With the advancement of intelligent algorithms, an increasing number of nonlinear
532 models have been employed in landslide displacement prediction. Additionally, investigating
533 the affecting triggering factor improves the quality of the dataset, reduces the randomness, and
534 decreases the computational effort (Han et al., 2021). Consequently, it is impractical to use
535 linear or empirical equations to simulate or predict dynamic, non-linear, and unsymmetrical
536 data (Lian et al., 2014; Yao et al., 2015). Intelligence models offer a viable way to manage such
537 dynamic relationships. Artificial intelligence models can be regression (Niu et al., 2021),
538 classification (supervised) (Tengtrairat et al., 2021), and clustering (unsupervised) (de Souza
539 & Ebecken, 2012; Lian et al., 2016). The application of supervised learning techniques is the
540 most prevalent in recent research articles (Ebrahim et al., 2024c). Intelligence regression
541 models can be used to predict displacement (Lian et al., 2014), groundwater level, and matric
542 suction (Davar et al., 2022). It can be combined with physical models to improve the model
543 performance (Marrapu et al., 2021), reduce uncertainty (Xing et al., 2019), and overcome
544 missing data issues (de Souza & Ebecken, 2012). Classification models were utilized to provide
545 landslide susceptibility maps (Tengtrairat et al., 2021). Artificial regression models were
546 mainly adopted for regional areas, such as physical models and empirical-statistical thresholds.
547 At the same time, classifications and landslide susceptibility (LSM) were mainly used for large
548 catchments to plan land usage (Oh & Lee, 2017). The regression intelligence model is discussed
549 first in this study (part i), and LSM is discussed afterward in part ii which has been published
550 (refer to (Ebrahim et al., 2024a). Figure 20 highlights the different recently adopted methods
551 regarding displacement prediction.

552 Thus, single artificial models have been adopted, such as ANN (BPNN) (de Souza &
553 Ebecken, 2012; Liu et al., 2016; Neupane & Achet, 2004), RNN (Yao et al., 2015), ELM (Yao
554 et al., 2015; Cao et al., 2016), GM(1,1) (Yao et al., 2015), SVM (Cao et al., 2016), RF (Krkac
555 et al., 2017; Krkač et al., 2020), and MLR (Krkac et al., 2020). However, these single models



556 may be improved due to the dynamic nature of landslides and their influencing factors (Lian et
557 al., 2014; Yao et al., 2015; Gao et al., 2020; Li et al., 2021). For example, landslide
558 displacement can be classified into trend and periodic behavior, as shown in Figure 21. The
559 former mainly depends on the creep effect of landslides, such as lithology, structure, and stress
560 state, while the latter is pertinent to random factors such as rainfall, reservoir level fluctuation,
561 and groundwater change. Predicting sudden changes in displacement has received much
562 interest due to its significant effect (Lian et al., 2016). Traditional models such as ANN and
563 SVM have low accuracy in predicting such behavior because the volume of such displacement
564 points (mutational points) is much lower than the trend point. Moreover, the periodic points are
565 always delayed with the triggering factor (Figure 22). Therefore, Gao et al. (2020) and Li et al.
566 (2021) recommended using multi-data-driven models to manage such complex behavior.

567 EEMD–ELM (Lian et al., 2014), LSTM-DMA (Xing et al., 2019), GM-ENN (Gao et al.,
568 2020), KGM, MKGW, and WMKGM (Li et al., 2021), WCA-BPNN (Zhang et al., 2021a),
569 SSA-LSTM (Yang et al., 2022), EEMD-RNN, EEMD-GRU, EEMD-LSTM, EEMD-SVM,
570 EMD-LSTM, and EEMD-ELM (Niu et al., 2021), ELM-RS-SVR (Wang et al., 2023a), SVM-
571 (MSI, BA, GWO, DA, WOA, GOA, SSA)-CEEMD (Zhang et al., 2021b), SVC-PSO-SVR
572 (Han et al., 2021), DES-VMD-(BLSTM, BGRU, BRNN), DES-(BLSTM, BGRU, BRNN)
573 (Wang et al., 2023b), and (GOA-GA-VMD)-GRA-(TempoVar-Transformer) (Ye et al., 2024)
574 were utilized to overcome the shortening of the single models. Hybrid models refer to a model
575 that combines the advantages of more than one model to surpass the drawbacks of a single
576 model.



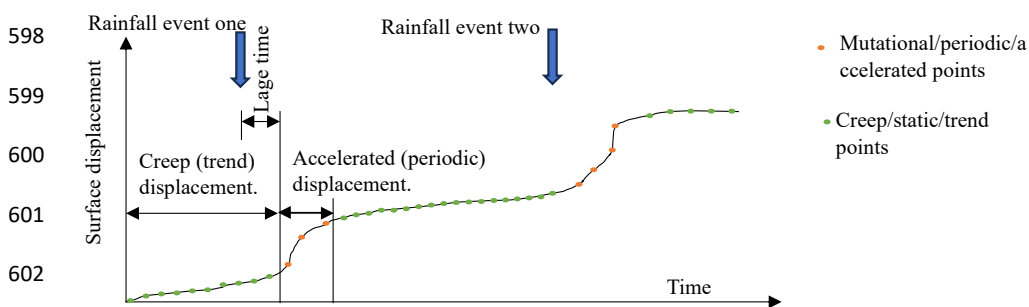
577

578 **Figure 20.** Model selection of landslide displacement.

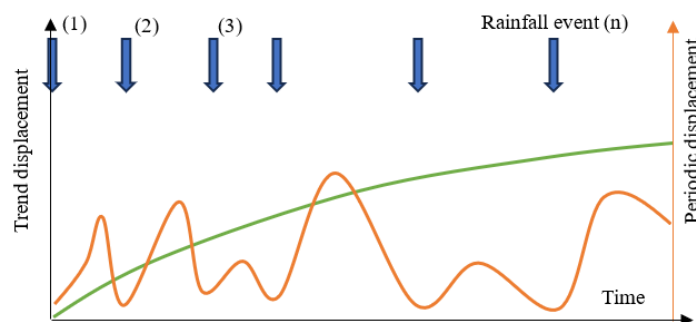


579 3. Model decomposition and data preparation.

580 As shown in Figure 22, the cumulative displacement can be separated into creep and
 581 accelerated displacement using various analysis techniques, including high-pass (HP) filter
 582 analysis (Zhang et al., 2021a), double moving average (DMA), and single moving average
 583 (SMA) models (Xing et al., 2019). Other methods include empirical mode decomposition
 584 (EMD) (Niu et al., 2021), ensemble empirical mode decomposition (EEMD) (Lian et al., 2014),
 585 EEMD with kurtosis criterion (Niu et al., 2021), and complete ensemble empirical mode
 586 decomposition (CEEMD) (Zhang et al., 2021b). The CEEMD mode has an advantage over
 587 EMD and EEMD that can consider the residual term of first decreasing and then increasing. A
 588 support vector classifier (SVC) can be used to classify the creep and acceleration state (Han et
 589 al., 2021). DES-BDNN (Wang et al., 2023b) and K-means clustering (Lian et al., 2016) were
 590 also adopted to divide the total displacement into stationary and mutational points. Variational
 591 mode decomposition (VMD) can be employed to isolate each displacement component, with
 592 optimization achieved through the GroupWise coupling algorithm (Ye et al., 2024). Following
 593 this, the cumulative predicted displacement is calculated by superimposing the results from
 594 both models. It is important to note that periodic displacement is predicted using factors such
 595 as rainfall, reservoir level, groundwater level, and periodic displacement itself. In contrast,
 596 trend displacement is forecasted using historical cumulative displacement data (Niu et al.,
 597 2021).



603 **Figure 21.** Accelerated and creep displacement points.

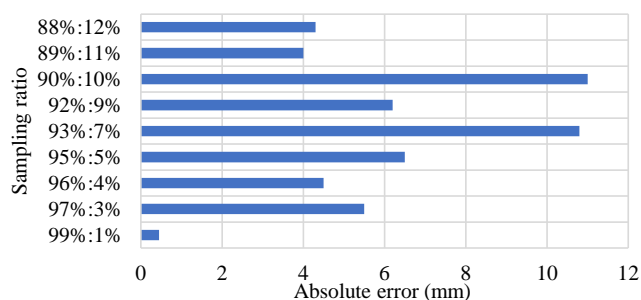


604

605 **Figure 22.** Trend and periodic displacement change according to a rainfall event.

606 4. Training and testing data split ratio.

607 Generally, the ratio of the training and testing datasets is a factor affecting the accuracy of the
608 prediction. Krkac et al. (2017) adopted different ratios and suggested that a testing ratio of up
609 to 4% is acceptable, as shown in Figure 23. Krkač et al. (2020) adopted 49 Folds with a training
610 ratio of 98% and a testing ratio of 2%. Wang et al. (2023b) utilized a new technique to reduce
611 the complexity of nonlinear displacement and expand the quantity of training data using VMD
612 and interpolation, respectively. Most of the mentioned studies in Table 6 divided the monitoring
613 data based on a specific period or number of fixed measurements. For comparison purposes, it
614 is suggested to calculate the ratio and round it up to $\pm 5\%$ if the ratio is not mentioned in the
615 article. Training to testing sampling ratios of 70%:30% (Yao et al., 2015; Liu et al., 2016; Gao
616 et al., 2020; Zhang et al., 2021a; Zhang et al., 2021b; Davar et al., 2022; Ye et al., 2024) and
617 80%:20% (Lian et al., 2014; Cao et al., 2016; Lian et al., 2016; Xing et al., 2019; Marrapu et
618 al., 2021; Yang et al., 2022) are mostly employed. This was followed by a sampling ratio of
619 85%:15% (Han et al., 2021; Niu et al., 2021), 90%:10% (Li et al., 2021; Wang et al., 2023a),
620 60%:40% (Sasahara, 2017), and 50%:50% (Neaupane & Achet, 2004).



621

622 **Figure 23.** Absolute error values versus different sampling ratios.

623 5. Missing data and training data shortage.

624 Monitoring surface displacement encounters complicated circumstances such as monitoring
625 device failure, data noise, and loss, resulting in low forecast accuracy (Shentu et al., 2022).

626 Additionally, computerized monitoring equipment is continuously exposed to the outdoor
627 environment, leading to inevitable issues such as deterioration, aging, power loss, and other
628 factors, all of which can result in missing monitoring data (Wang & Zhao, 2023). Some
629 researchers have attempted to remove these missing data to create a complex intelligence model
630 (de Souza & Ebecken, 2012), use a small dataset (Shentu et al., 2022), adopt statistical filling
631 for missing data series (Li et al., 2021; Wang & Zhao, 2023), and utilize fusion transfer learning
632 (Long et al., 2022).

633 de Souza and Ebecken (2012) utilized artificial neural networks ANN combined with
634 statistical means (correlation and principal component analysis PCA) and clustering (K-means
635 and Dendrogram approaches) to predict rainfall missing data where PCA and correlation
636 combined with ANN achieved the best results. Shentu et al. (2022) adopted a small sampling
637 dataset using a new multivariate grey model (Feedback Optimizing Background Grey Model
638 FOBGM (1, N)) to predict the deep displacement. The proposed model achieved the best
639 accuracy compared with GM (1,1), GM (1, N), OGM (1, N), and BPNN. However, this study
640 neglects the actual complex conditions, as it is based on laboratory tests. Moreover, using a



641 small-sample dataset is not an ideal solution (Wang & Zhao, 2023). They propose a time series
642 prediction model for landslide displacement based on mean-based low-rank autoregressive
643 tensor completion (MLATC), which addresses the issue of missing data during the landslide
644 monitoring process. Li et al. (2021) applied cubic spline interpolation to handle data gaps, used
645 Savitzky-Golay filters to smooth noisy data, and employed the t-test to remove misfits. A novel
646 technique for handling missing data is proposed by Long et al. (2022), which assumes that
647 landslides in similar geographical and geological settings share similar deformation properties,
648 though they vary in magnitude. In this context, multi-feature fusion transfer learning (MFTL)
649 is used to incorporate data from neighboring locations with similar displacement behavior as a
650 training dataset. This approach provides a viable solution when a sufficient training dataset is
651 lacking. The dataset considered factors such as rainfall and reservoir level fluctuations to
652 predict mutation and creep displacements. Additionally, for mutation displacement, the non-
653 uniform weight error (NWE) was combined with MFTL to improve prediction accuracy.

654 6. Regression performance implementation.

655 To evaluate model accuracy, the most commonly used methods for displacement prediction
656 models include the coefficient of determination (R^2) and root mean squared error (RMSE).
657 Additionally, various other evaluation metrics, such as mean absolute error (MAE) and mean
658 squared error (MSE), are also employed. These parameters can be calculated using equations
659 9, 10, 11, and 12 (Willmott & Matsuura, 2005). Higher values of these parameters indicate
660 poorer model predictions, whereas values closer to 0 indicate higher accuracy. Moreover, the
661 standard deviation ratio (SDR) can be used to evaluate the model where the closest SDR to 0
662 highlights high accuracy (Bland & Altman, 1996). Pearson-R Correlation (PRC) assumes that
663 the values should fall between -1 and +1, where +1 denotes the strongest possible positive
664 agreement (Cohen, 1998).



$$9) R^2 = 1 - \frac{\sum_{i=1}^N (X_i - Y_i)^2}{\sum_{i=1}^N (Y_i - \bar{Y})^2} \qquad 10) RMSE = \sqrt{\frac{1}{N} \sum_{i=1}^N (X_i - Y_i)^2}$$
$$11) MAE = \frac{1}{N} \sum_{i=1}^N |X_i - Y_i| \qquad 12) MSE = (RMSE)^2$$

Where Y_i is the specific value of the i^{th} real data; \bar{Y} is the average value of the real data; X_i is the specific value of the i^{th} predicted data.

665 7. Displacement models prediction accuracy.

666 The performance of a prediction model is influenced not only by the intelligence of the model
667 itself but also by the underlying controlling factors. Landslide issues, for instance, have been
668 extensively studied through physical models, where the theoretical relationship between input
669 and output parameters is already established. Thus, if the input parameters in an intelligent
670 model correspond to the physical features, the output should ideally align with that of the
671 physical model (i.e., analytical models). The effectiveness of statistical or intelligent models is
672 largely determined by controlling factors, such as the strong dependence between the model
673 and these factors, the quality of the dataset, the sampling ratio, and the accuracy of the
674 inventory data. Table 6 provides a detailed comparison of these models, considering both their
675 final accuracy and performance. Additionally, Figures 24, 25, and 26 present a comparison
676 focused solely on the accuracy and performance of the models, emphasizing those with the best
677 results. The structure of this discussion is designed to offer insights into the controlling factors
678 and initial conditions influencing the models.

679 In general, there is no universally superior model; rather, the best prediction depends on
680 the investigation of the influencing features and the consideration of the actual initial
681 conditions, which can significantly enhance model accuracy (refer to Figure 21) (Han et al.,
682 2021; Dal Seno et al., 2024). Consequently, outdated or irrelevant features can negatively
683 impact the model, making it beneficial to remove these factors (Cao et al., 2016). Studies have



684 indicated that BPNN (Liu et al., 2016) and MLR (Krkač et al., 2020) offer reasonable accuracy;
685 however, these models are relatively simple and fail to capture dynamic and non-linear
686 relationships. This limitation arises because the well-established datasets often closely
687 represent the physical mechanisms (Krkač et al., 2020; Liu et al., 2016). Marrapu et al. (2021)
688 found that ANNs trained on large datasets tend to deliver higher accuracy compared to those
689 trained on smaller datasets. However, when the dataset lacks critical information, the model
690 needs to be refined to better understand these complex relationships (Zhang et al., 2021a). A
691 solid understanding of the physical behavior and initial conditions is essential for selecting the
692 most appropriate model. For instance, Wang et al. (2023a) categorized displacement into trend
693 and periodic datasets, which helps in selecting a more suitable model.

694 Disregarding the influence of the dataset, sampling ratio, and model assumptions, Figures
695 24, 25, and 26 emphasize the accuracy of various models, specifically in terms of root mean
696 square error (RMSE) and coefficient of determination (R^2). All data are provided in Table 6 for
697 further information. GM (1,1) achieved the minimum RMSE among all single models for total
698 displacement. At the same time, PSO-SVR-SVC hit the minimum RMSE among all hybrid
699 models. The maximum R^2 can be achieved for creep displacement by adopting simple
700 polynomial regression, while the minimum RMSE is recorded using the LSTM-DMA hybrid
701 model. Regarding periodic displacement, RS-SVR records the maximum R^2 and hits the
702 minimum RMSE. Generally, trend displacement can be predicted using a simple polynomial
703 regression (Zhang et al., 2021a; Wang et al., 2023a), a grey model (Gao et al., 2020), or a single
704 artificial intelligence model such as ELM (Wang et al., 2023a) and DES (Wang et al., 2023b).
705 These models provide high accuracy for trend displacement. However, the problem is a
706 periodic displacement that exhibits complex and non-linear behavior (Gao et al., 2020; Li et
707 al., 2021). The short-term acceleration effect displacement (Periodic) requires hybrid model
708 analysis such as RS-SVR.

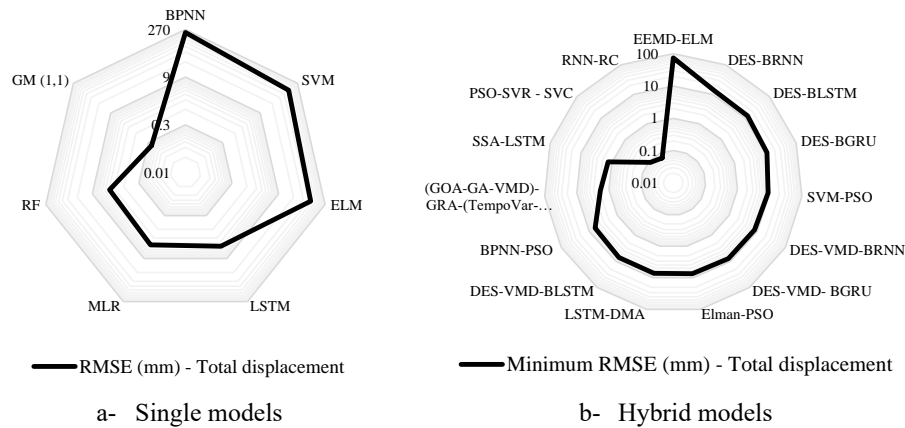


Figure 24. Comparison between different models' accuracy according to RMSE.

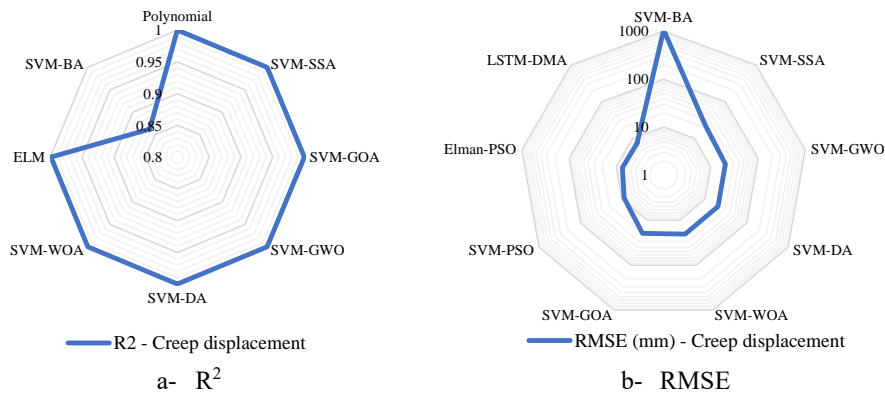


Figure 25. Comparison between different creep models' accuracy.

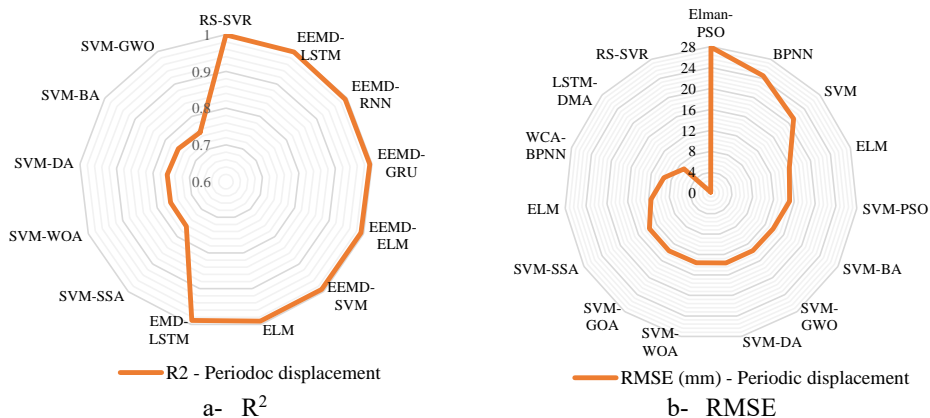


Figure 26. Comparison between different periodic models' accuracy.



710 **Table 6.** Recent artificial intelligence models predict landslide displacement.

Study	Key features	Model with the best accuracy			Sampling ratio (Training: Testing)	Model performance: (R^2) ¹ , RMSE (mm) ² , MAPE% ³ , MSE (mm ²) ⁴ , Minimum error% ⁵ , Maximum error % ⁶ , MAE (mm) ⁷ , MAPE (mm) ⁸	
		Creep	Periodic	Decomposition		Creep displacement	Periodic displacement
(Neaupane & Achet, 2004; Yao et al., 2015; Cao et al., 2016; Liu et al., 2016; Krkač et al., 2017; Krkač et al., 2020; Li et al., 2021; Yang et al., 2022)	- Trend features: Time series cumulative displacement. - Periodic features: Antecedent, rolling, and current data for rainfall, reservoir level, and groundwater level. - Infiltration and evaporation data to estimate effective rainfall*.				- Varied sampling ratio (refer to Section 4.2.1.4) - 70%:30% and 80%:20% are widely adopted		
(Lian et al., 2014; Gao et al., 2020; Xing et al., 2019; Niu et al., 2021; Zhang et al., 2021a; Zhang et al., 2021b; Han et al., 2021; Wang et al., 2023a; Wang et al., 2023b; Ye et al., 2024)							

711 *Matric Suction and Groundwater Prediction.*

712 Artificial intelligence models can also be employed to predict internal causative factors, such as
 713 soil matric suction (SMS) and groundwater levels, due to their non-linear and complex nature. In
 714 this context, SMS, which can represent soil shear strength, was predicted using a hybrid
 715 intelligence model developed by Davar et al. (2022). This hybrid model not only incorporates
 716 extensive datasets of physical soil properties but also evaluates the effects of three different
 717 algorithms: Bayesian Regularization Backpropagation (BR-BP), Particle Swarm Optimization
 718 (PSO), and Butterfly ANN Optimization Algorithm (BOA). The proposed hybrid model addresses
 719 the slow learning rate and generalization issues often associated with ANN models. The study
 720 utilized comprehensive field monitoring and laboratory data, including soil depth, VSMC, air



721 temperature, rainfall, soil temperature, and suction. Among the various models, PSO-ANN
722 demonstrated the best performance.

723 Similarly, groundwater level fluctuations are closely linked to landslide occurrences, with
724 the behavior of groundwater being influenced by rainfall and reservoir level fluctuations, albeit
725 with a time lag. Cao et al. (2020) applied a hybrid model known as the Genetic Algorithm-Support
726 Vector Machine (GA-SVM) to address the nonlinearity between intrinsic and extrinsic factors. The
727 model incorporated multiple features, including antecedent and current rainfall and reservoir
728 levels. The results showed that the accuracy of the GA-SVM model exceeded that of the BPNN
729 model. However, both the GA-SVM and BPNN models with multi-features outperformed the GA-
730 SVM model with a single feature. Liu et al. (2021) employed a regression tree model to predict
731 groundwater level changes, using rainfall, soil moisture content, and water level as input
732 parameters. The soil moisture content takes into account various factors such as surface runoff,
733 vegetation, climate conditions, and soil structure. The proposed model outperformed ANN, SVM,
734 ELM, and Gaussian Process Regression (GPR), achieving an RMSE of 0.0812. Ng et al. (2023)
735 introduced a novel multivariate long short-term memory (M-LSTM) model to predict pore water
736 pressure (PWP) responses by simultaneously utilizing spatial and temporal PWP data from
737 multiple measurement locations. However, such models are limited by the lack of geotechnical
738 data, whereas displacement prediction is more widely adopted due to the availability of monitoring
739 data for surface displacement.

740 *Moisture Content and Topographic Thresholds.*

741 Zhao et al. (2019b) incorporated the effect of antecedent soil moisture content along with recent
742 rainfall using a Bayesian probabilistic approach. The soil moisture content was calculated using
743 the SHETRAN (Système Hydrologique Européen TRANsport) model. The rainfall event,



744 antecedent soil wetness, rainfall duration, cumulative rainfall (mm), and landslide were examples
745 of the datasets used in the Bayesian analysis. Thus, probabilistic thresholds can provide better
746 accuracy than I-D thresholds. De Luca and Versace (2017) utilized the new GFM (Generalized
747 FLaiR Model), which can be used for both shallow and deep-seated landslides. The GFM considers
748 the initial soil moisture that depends on antecedent rainfall. Additionally, several configurations
749 can be defined to choose the most suitable threshold, as illustrated in Equations 13 and 14. A
750 lumped conceptual hydrological model is used to develop a threshold (Equation 15). The
751 production storage level (PSL) is calibrated using evaporation and discharge data, accounting for
752 the wetness increase throughout the entire event (WI) (Bezak et al., 2019). This model was
753 developed based on the GR4J model, as adapted from Perrin et al. (2003) (refer to Figure 27). The
754 $R - PSL$ threshold produces meaningful results compared to $I-D$ thresholds for long-duration
755 rainfall, while for events with different characteristics, such as short duration, other definitions,
756 such as hourly rainfall data, are used instead of daily rainfall (Bezak et al., 2019).

757 **13)**
$$Y(t) = \int_{t-M}^t I(T)\Xi(t-T)dT$$

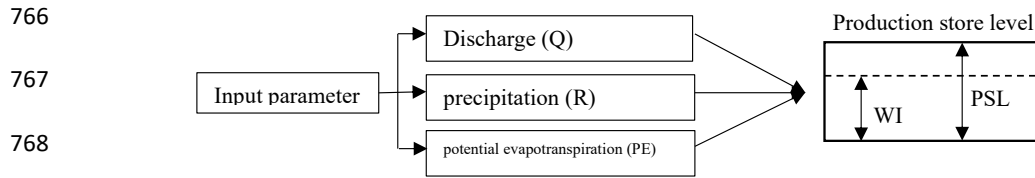
758 **14)**
$$Y_{\sigma}(t) = (R_D^*(t-d)/D) + (f[R_D^*(t-d)]/d)$$

759 **15)**
$$R = a * PSL + b$$

760 where Y is a mobility function, I is rainfall intensity, Ξ represents a filter function that can
761 take different mathematical expressions, t is time, T is defined on the interval $[t-M; t]$, M is the
762 process's temporal memory, and R_D^* is cumulative rainfall filtered on D and d durations and
763 evaluated at the instants $(t-d)$ and t , respectively.

764

765

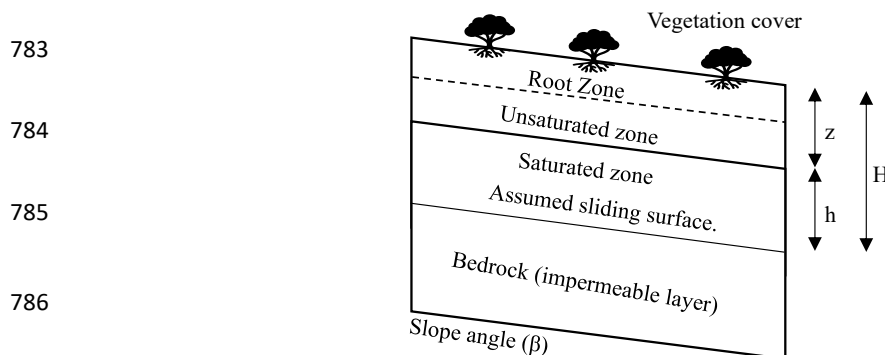


769 **Figure 27.** GR4J model.

770 The saturation storage of the soil, as described by Lee and Ho (2009), is illustrated in Figure
 771 28. The soil thickness above the bedrock (H) is divided into the unsaturated zone (z) and the
 772 saturated zone (h). When the cumulative rainfall exceeds the water storage capacity of the
 773 unsaturated zone, the depth of the saturated zone increases. Full saturation of the soil layer occurs
 774 when the rainfall reaches from the ground level to the bedrock level (Cho, 2017). As a result, the
 775 saturated thickness can be calculated using Equation 16 (Ho & Lee, 2017). Additionally,
 776 topography plays a crucial role, and a wetness index proposed by Kirkby (1975) is used to describe
 777 the spatial distribution of the surface soil, as shown in Equation 17. Therefore, thresholds can be
 778 concluded based on these assumptions illustrated in Equations 18 and 19 (Ho et al., 2012).

779 **16)**
$$h(t) = H - Z(t) - FRC \left[ATI - \ln \left(\frac{W}{\tan \beta} \right) \right]$$

780 Where $h(t)$ denotes the saturated water height at time t , H represents the soil thickness, W is
 781 the unit width collecting area, $\tan \beta$ is the surface slope, and ATI refers to the average topographic
 782 index in the catchment. FRC is a model coefficient obtained through the flow recession records.



787 **Figure 28.** The coupled hydrological-slope instability model.



788 **17)** $TWI = \ln(W / \tan \beta)$

789 **18)** $\tan \beta \geq \left[\frac{C}{\gamma_i g H \cos^2 \beta} + \tan \phi \right]$ lower thresholds

790 **19)** $\tan \beta < \left[\frac{C}{\gamma_i g H \cos^2 \beta} + \left(1 - \frac{\gamma_w}{\gamma_i} \right) \tan \phi \right]$ upper thresholds

791 Since C denotes the cohesion, g represents the gravitational acceleration, γ_i is the bulk
792 density of the soil, γ_w is the density of water, H is the soil thickness measured vertically, β is the
793 gradient of the hill slope, and ϕ is the angle of the soil's effective friction.

794 It is assumed that soil moisture content can be correlated with the topographic wetness index
795 (TWI) during wet conditions (Wang et al., 2020). The TWI is used to represent the spatial
796 distribution of surface soil using digital elevation models (DEMs) (Lee & Ho, 2009; Ho et al.,
797 2012; Ho & Lee, 2017). A high-resolution DEM helps reduce uncertainties in slope geometry
798 (Valentino et al., 2014). Consequently, soil thickness is essential for performing instability analysis
799 (Lee & Ho, 2009; Ho et al., 2012; Wang et al., 2016; Cho, 2017; Ho & Lee, 2017; Wang et al.,
800 2020). In contrast to the TWI, the soil wetness index (SWI) is influenced by rainfall conditions
801 (Rodrigues Neto et al., 2023). This factor accounts for soil moisture conditions, which are crucial
802 in determining the occurrence of landslides (Zhao et al., 2020). Using hydrological models, the
803 Soil Wetness Index (SWI) can be estimated, allowing for the development of SWI thresholds.
804 Additionally, SHETRAN is a finite difference hydrological model based on partial differential
805 equations for flow and transport, solved in a three-dimensional grid (Birkinshaw & Ewen, 2000).
806 This model is particularly effective in simulating soil moisture responses to rainfall. SHETRAN
807 considers meteorological conditions such as potential evapotranspiration and precipitation and
808 topographic properties such as TWI. Additionally, land cover and soil type were considered. This
809 method counts for antecedent conditions, not only for current conditions. The Soil Wetness Index



810 (SWI) is calculated using the rainfall data from the previous day of a rainfall event, with average
811 values taken from all meteorological stations. The SWI for the last day of the rainfall event in a
812 warning zone is calculated for each grid cell within that zone. This value is then compared to a
813 predefined soil wetness threshold. If the SWI exceeds the threshold, the corresponding grid cell is
814 classified as being wet (Zhao et al., 2020).

815 **DISCUSSION**

816 Empirical-statistical thresholds were built, assuming that rainfall is the most critical causative
817 feature for landslide occurrence (Hong et al., 2018). This assumption can be advantageous if
818 topographic, geotechnical, and hydraulic elements are lacking. These models do not need slope-
819 mounted measurement equipment (Ering & Babu, 2020). Due to their simplicity, empirical models
820 are preferred for early warning systems (EWS) (De Luca & Versace, 2017). These thresholds
821 provide a simpler alternative to the complex procedures involved in physically based models,
822 which require extensive data monitoring, collection, and model calibration. As a result, physically
823 based models are seldom used in operational Early Warning Systems (EWS) (Bezak et al., 2019).
824 However, a notable constraint of these thresholds is the limited usage for a specific case study
825 (Huang et al., 2015). With limited data on rainfall and landslide occurrences, empirically based
826 models struggle to provide accurate rainfall thresholds (Pagano et al., 2010; Wu et al., 2015). While
827 these thresholds can achieve high accuracy, their forecasting capability is often limited by a
828 significant proportion of false positive alarms (Hong et al., 2018; Uwihirwe et al., 2020).

829 Physically based causative thresholds are constructed based on certain assumptions,
830 assuming that the relationship between landslides and the controlling feature factors will remain
831 relatively constant in the future (Krkač et al., 2017). In essence, these models operate under the
832 assumption that past events will recur in the future without notable changes and that sudden



833 failures, such as strain softening along the sliding surface, will not take place. As sudden failures
834 are seldom included in training datasets, these models lack the ability to predict such events. As a
835 result, any factors absent from the training data remain beyond the scope of prediction (Xing et
836 al., 2019; Zhang et al., 2021b). These models neglect random events due to the lack of monitoring
837 data and rarely available data, such as wind and vehicle loads (Wang et al., 2023a). Additionally,
838 these models have some limitations: The prediction accuracy depends on the prediction step,
839 whereas better accuracy comes from the small-step prediction (Gao et al., 2020). Regression
840 models, unlike landslide susceptibility maps, are generally more suited for smaller areas due to
841 their dependency on field monitoring data. Causative thresholds often concentrate on a single
842 parameter, such as displacement or groundwater levels, while overlooking essential factors like
843 spatial variations in land cover, soil composition, topography, and geotechnical or hydrological
844 attributes. Moreover, most of these models are limited to historical data for training, restricting
845 their ability to provide real-time predictions or adapt to sudden changes (Liu et al., 2021). Despite
846 these limitations, these models have notable advantages. Artificial intelligence models, for
847 instance, can analyze multiple causative factors using existing monitoring data, delivering
848 extended warning periods compared to theoretical models and greater accuracy than empirical-
849 statistical thresholds. Furthermore, they are a cost-effective alternative for landslide prediction, as
850 they require minimal geotechnical investigation.

851 Figure 29 presents a comprehensive framework for modeling landslides across local and
852 national scales. The flowchart delineates a clear, structured progression from macroscopic models
853 focused on a national-scale landslide to more localized models, offering fine-tuned, detailed
854 insights on a regional basis. These modeling approaches reflect a hierarchical decision-making



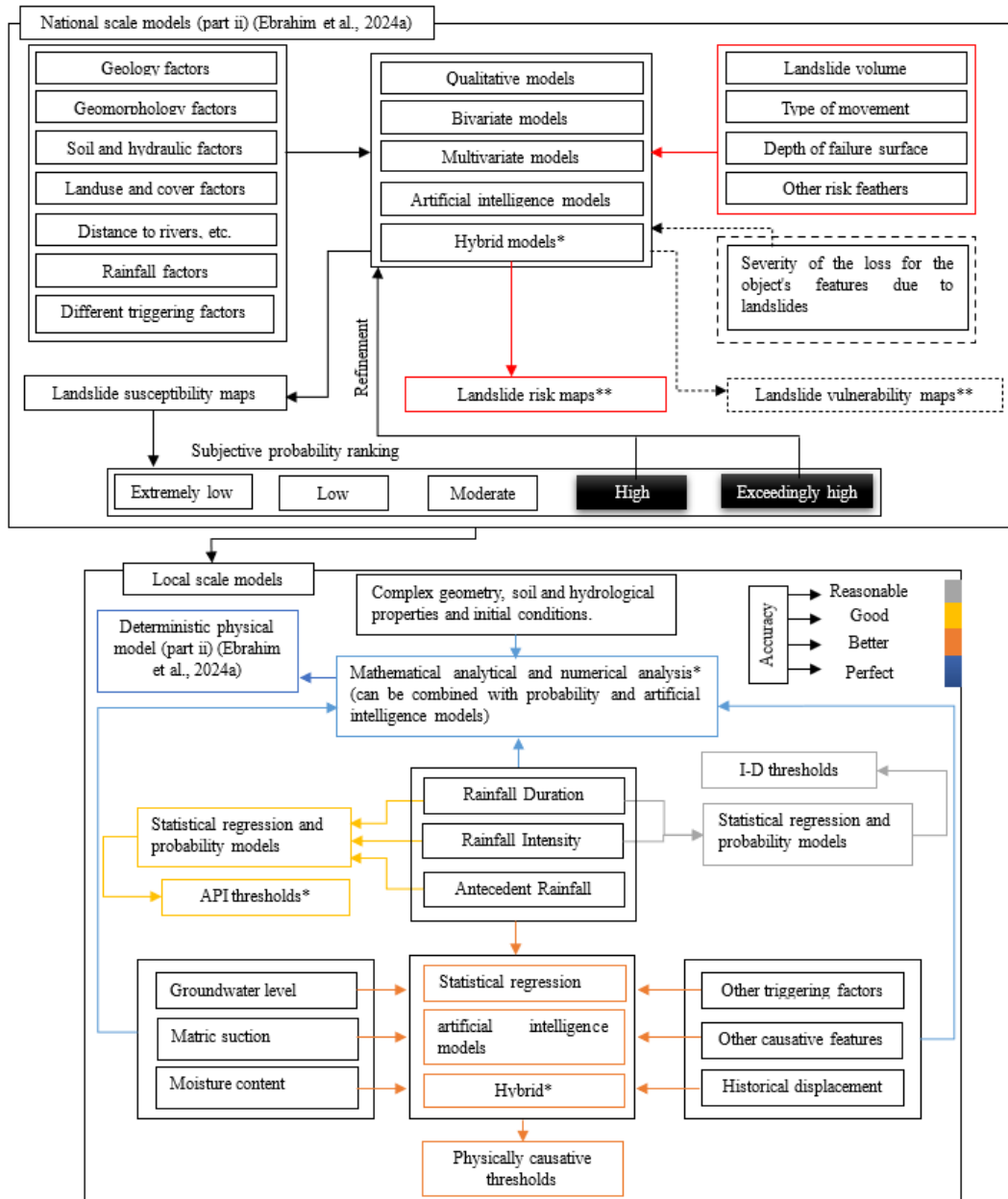
855 process where different input parameters, ranging from geological factors to rainfall intensity,
856 guide the selection of the most appropriate model type.

857 At the national scale (refer to part ii (Ebrahim et al., 2024a)), the framework demonstrates
858 how factors like geology, geomorphology, soil, and hydraulic properties, along with triggering
859 factors such as rainfall, lead to the generation of landslide susceptibility maps. These maps serve
860 as the foundation for risk assessments using multivariate models, AI techniques, and hybrid
861 approaches. These elements allow for the precise identification of areas with high risk and the
862 corresponding impacts on infrastructure and human life (refer to Ebrahim et al. (2024a) for more
863 insights).

864 Transitioning to the local scale, the framework shifts to more detailed models that account
865 for complex geometrical, hydrological, and soil conditions. Here, the integration of physical,
866 mathematical, and AI models becomes essential. Deterministic physical models take the lead,
867 simulating intricate landslide processes by considering site-specific conditions (refer to part ii
868 (Ebrahim et al., 2024a)). Statistical regression, AI, and probabilistic models complement these
869 physical responses, offering insights into landslide initiation based on landslide response such as
870 displacement, groundwater levels, matric suction, or moisture content. These models, in
871 combination with I-D thresholds (rainfall intensity-duration), help forecast landslide initiation with
872 increasing accuracy. One of the most innovative aspects of Figure 29 is its representation of hybrid
873 modeling approaches, where the strengths of different methods, such as statistical regression, AI,
874 and physical models, are combined. This integrated approach is essential for improving predictive
875 accuracy in complex scenarios, especially in rainfall-induced landslide studies. The API threshold
876 analysis, for example, stands out as a novel way of incorporating antecedent rainfall information
877 to refine early warning systems. Accuracy assessment, represented through color codes



878 (reasonable, good, better, perfect), reflects the refinement and calibration of models. This visual
879 representation is essential for researchers as it offers a quick assessment of model reliability based
880 on specific input conditions. This multi-tiered approach is fundamental for developing more robust
881 predictive frameworks that can be tailored to different geographic scales, from national
882 susceptibility mapping to site-specific, highly accurate risk assessments.



883

884 **Figure 29.** Various prediction models with their respective accuracy, input parameters, and
 885 analysis techniques (Ebrahim et al., 2024a). * denotes the model with the best accuracy, and **
 886 indicates out-of-scope models.



887 **CONCLUSIONS AND FUTURE WORK.**

888 This study combined both quantitative (scientometric) and qualitative (systematic) analyses. The
889 scientometric approach is an effective method for addressing the challenges of manual searches by
890 highlighting the most significant contributions from keywords, authors, institutions, and countries.
891 The main finding is that landslide prediction models have evolved significantly over the past
892 decade, reflecting the growing global concern for reducing the loss of lives and financial resources.
893 The journal "Landslides" stands out as the most frequently published and cited. China leads in
894 terms of publications, citations, and international collaboration. The most-cited article, based on
895 both total and normalized citations, is by Merghadi et al. (2020). The most common keywords
896 include "Landslides," "Landslide," "rain," "forecasting," and "rainfall.

897 This study showcased the latest advancements and cutting-edge landslide prediction models,
898 including both empirical statistical thresholds and physically based causative thresholds. When
899 only rainfall data are available, empirical thresholds (I-D thresholds) can give good accuracy while
900 having a significant false positive rate. Recently, because antecedent rainfall can effectively imitate
901 the initial moisture content of the soil, API thresholds are more accurate than I-D thresholds. API
902 criteria not only improve accuracy but also lower the number of incorrect predictions. Statistical
903 regression or probability analysis approaches can be used to create these criteria. However, these
904 thresholds are far from the physical mechanism of the slope itself. It can be adopted when the
905 physical input parameters are lacking.

906 Consequently, physically based causative thresholds correlate external rainfall-triggering
907 factors with any internal slope feature, such as displacement, soil moisture, suction stress, and
908 groundwater level. Displacement thresholds have been widely investigated due to the availability
909 of their input data, while other causative features are lacking due to their dependency on the



910 geotechnical and hydrological parameters. Statistical regression models can be used to predict
911 displacement. These models, however, failed to predict the sudden increased displacement. Single
912 artificial intelligence models have recently been adopted for complicated issues. These models
913 have acceptable accuracy but are unable to anticipate periodic displacement. As a result, recent
914 studies have divided displacement into trend and periodic terms. Polynomial or basic artificial
915 intelligence models can be used to forecast trend displacement. On the other hand, periodic
916 displacement can be precisely anticipated by utilizing hybrid artificial intelligence models.
917 Furthermore, hybrid models can deal with missing data and a lack of training data. Nonetheless,
918 these models cannot predict any variable outside the training dataset, lack sophisticated initial
919 conditions, and ignore slope geometry.

920 **Future Directions and Recommendations.**

921 High-accuracy models can be achieved by considering two key factors: 1) choosing the appropriate
922 features based on a deeper understanding of the case study's initial conditions, and 2) selecting a
923 suitable model to capture the relationship between these features. Despite advancements in
924 statistical modeling, such as hybrid AI models, there are still some gaps that need to be addressed,
925 as outlined in Table 7.

926 **Table 7.** Research gaps in landslide prediction models (I-D thresholds and physically based
927 causative thresholds)

Gap	Recommendations
I-D thresholds suffer from a high false prediction rate. This can be illuminated because of two reasons: 1) I-D thresholds neglect the vegetation cover that affects the rate of the infiltration and the subsurface water content; and 2) I-D thresholds	Field tests shall be performed to build the relationship between rainfall, evaporation, infiltration, and surface runoff. Sensitivity analysis shall be performed to select the optimum physical properties that achieve better accuracy. This may reduce the false prediction rate



neglect the slope properties (geometry, geotechnical properties, etc.)	and keep the advantages of the I-D thresholds as a simple technique.
Physically based causative thresholds rely mainly on surface characteristics (i.e., surface displacement) neglecting the sudden failure scenario. This can be explained by the issue of the available data. In other words, the prediction models that consider the actual subsurface mechanism of landslide (i.e., tilting, suction stresses, groundwater variation, deep displacement, etc.) are lacking.	Monitoring of subsurface characteristics provides a well-established dataset to be used afterward to predict the complex mechanism of the landslide using hybrid AI models. This may overcome the limitation of the available models and may help better understand landslide non-linear complex mechanisms.
Most studies neglect the effect of the harsh environment such as data loss. Additionally neglects the effect of the communication issue such as the data rate.	A sensitivity analysis shall be developed to investigate and optimize the data rate and model selection considering the issue of data loss.

928 **DECLARATIONS**

929 **Availability of Data and Materials**

930 The data presented in this article were either provided in tables as examples or can be found in the
931 cited references.

932 **Competing Interests**

933 The authors declare no competing interests.

934 **Funding**

935 There was no funding provided for this research.

936 **Authors' Contributions**

937 Conceptualization, K.M.P.E., and T.Z.; methodology, K.M.P.E., and T.Z.; formal analysis,
938 K.M.P.E., S.M.M.H.G., T.Z., and G.A.; investigation, K.M.P.E., and T.Z.; resources, T.Z.; data
939 curation, K.M.P.E., S.M.M.H.G., T.Z., and G.A.; writing— original draft preparation, K.M.P.E.;
940 writing—review and editing, S.M.M.H.G., T.Z., and G.A.; supervision, T.Z. All authors have read
941 and agreed to the published version of the manuscript.



942 **Acknowledgments**

943 The authors gratefully acknowledge the Innovation and Technology Support Programme (ITSP)
 944 [Grant No. ITS/033/20FP], Hong Kong SAR. The authors would like to thank the Head of the
 945 Geotechnical Engineering Office, the Government of the Hong Kong SAR, for the permission to
 946 use Figure 10. The authors gratefully acknowledge the fund provided by the Hong Kong
 947 Polytechnic University.

948 **Declaration of generative AI and AI-Assisted Technologies in The Writing Process**

949 During the preparation of this work, the author(s) used [GPT 3.5] to [rephrase, check grammar and
 950 spelling]. After using this tool/service, the author(s) reviewed and edited the content as needed and
 951 take(s) full responsibility for the content of the publication.

952 **NOTATION AND ABBREVIATIONS**

953 **Table 8.** Notation

D	Rainfall duration	ε	Scaling parameter
I	Rainfall intensity	ζ	Shape parameter
E_N	Rainfall event,	v	Dimensionless parameter
API_N	Antecedent precipitation index	Y_i	Value of real data
N	Number of rainy days	X_i	Value of predicted data
R_a	Antecedent rainfall	C	Cohesion
R_o	Rolling rainfall	ϕ	Internal friction angle
R	Cumulative rainfall	Q	Discharge
PE	Potential evaporation	g	Gravitational acceleration
S	Displacement	γ_w	The unit weight of water
$E(t)$	Gamma-type transfer function	γ_t	Wet unit weight
t	time	H	Thickness above the bedrock layer
T	Temporal scale/Time intervals	z	Unsaturated thickness
M	Temporal memory	h	Saturated thickness

954 **Table 9.** Abbreviation

EWS	Early warning systems	GRU	Gated recurrent unite
$FLaIR$	Forecasting of Landslides Induced by Rainfall	$BRNN$	Bayesian recurrent neural network
GFM	Generalized FLaIR model	$BLSTM$	Bayesian long short-term memory network
$IETDs$	Inter-event time definitions	$BGRU$	Bayesian gated recurrent unit network
SMS	Soil matric suction	$BDNN$	Bayesian deep neural networks
$VSMC$	Volumetric soil moisture content	EMD	Empirical mode decomposition
PSL	Production storage level	$EEMD$	Ensemble empirical mode decomposition
WI	Wetness increase	$CEEMD$	Complete ensemble empirical mode decomposition



<i>TWI</i>	Topographic witness Index	<i>DMA</i>	Double moving average
<i>SWI</i>	Soil wetness index	<i>SMA</i>	Single moving average
<i>SHETRAN</i>	Système Hydrologique Européen TRANsport	<i>DES</i>	Double exponential smoothing
<i>AUC</i>	The area under the ROC curve	<i>VMD</i>	Variational mode decomposition
<i>ROC</i>	Receiver operating characteristic	<i>KGM</i>	Kernel-based grey model
<i>FPR</i>	False positive rate	<i>MKGM</i>	Multi-kernel grey model
<i>R²</i>	Coefficient of determination	<i>WMKGM</i>	Weighted multi-kernel grey model
<i>RMSE</i>	Root mean square error	<i>WCA</i>	Water cycle algorithm
<i>MSE</i>	Mean square error	<i>MSI</i>	Multiple Swarm intelligence
<i>MAE</i>	Mean absolute error	<i>BA</i>	Bat algorithm
<i>SDR</i>	Standard deviation ratio	<i>GWO</i>	Grey wolf optimization
<i>PRC</i>	Pearson-R correlation	<i>DA</i>	Dragonfly optimization algorithm
<i>GM</i>	Grey model	<i>WOA</i>	Whale optimization algorithm
<i>MLR</i>	Multilinear regression	<i>GOA</i>	Grasshopper optimization algorithm
<i>ANN</i>	Artificial neural networks	<i>SSA</i>	Sparrow search algorithm
<i>BPNN</i>	Backpropagation neural networks	<i>PCA</i>	Principal component analysis
<i>SVM</i>	Support vector mechanism	<i>FOBGM</i>	Feedback optimization background grey model
<i>RF</i>	Random forest model	<i>MLATC</i>	Mean-based low-rank autoregressive tensor completion
<i>SVC</i>	Support vector classifier	<i>MFTL</i>	Multi-fusion transfer learning
<i>SVR</i>	Support vector regression	<i>NWE</i>	Non-uniform weight error
<i>RS</i>	Random Search	<i>BR-BP</i>	Bayesian regularization backpropagation
<i>RNN</i>	Recurrent neural networks	<i>BOA</i>	Butterfly optimization Algorithm
<i>ENN</i>	Evolutionary neural network	<i>GA</i>	Genetic algorithm
<i>ELM</i>	Extreme learning machine	<i>GPR</i>	Gaussian process regression
<i>LSTM</i>	Long short-term memory	<i>GRA</i>	Grey correlation analysis
<i>VMD</i>	Variational Mode Decomposition	<i>GA</i>	Genetic algorithm

955 REFERENCES

- Abolmasov, B., Milenković, S., Marjanović, M., Đurić, U., & Jelisavac, B. (2015). A geotechnical model of the Umka landslide with reference to landslides in weathered Neogene marls in Serbia. *Landslides*, 12(4), 689-702. <https://doi.org/10.1007/s10346-014-0499-4>.
- Aryastana, P., Dewi, L., & Wahyuni, P. I. (2024). A study of rainfall thresholds for landslides in Badung Regency using satellite-derived rainfall grid datasets. *Int J Adv Appl Sci*, 13(2), 197-208. <https://doi.org/10.11591/ijaas.v13.i2.pp197-208>
- Baum, R. L., Savage, W. Z., & Godt, J. W. (2008). TRIGRS: a Fortran program for transient rainfall infiltration and grid-based regional slope-stability analysis, version 2.0. U.S. Geological Survey Open-File Report, 1159.
- Bednarczyk, Z. (2018). Identification of flysch landslide triggers using conventional and 'nearly real-time monitoring methods—An example from the Carpathian Mountains, Poland. *Engineering Geology*, 244, 41-56. <https://doi.org/10.1016/j.enggeo.2018.07.012>.
- Bezák, N., Jemec Auflič, M., & Mikoš, M. (2019). Application of hydrological modelling for temporal prediction of rainfall-induced shallow landslides. *Landslides*, 16(7), 1273-1283. <https://doi.org/10.1007/s10346-019-01169-9>.
- Birkinshaw, S. J., & Ewen, J. (2000). Nitrogen transformation component for SHETRAN catchment nitrate transport modelling. *Journal of Hydrology*, 230(1-2), 1-17. [https://doi.org/10.1016/S0022-1694\(00\)00174-8](https://doi.org/10.1016/S0022-1694(00)00174-8).
- Bland, J. M., & Altman, D. G. (1996). Statistics notes: measurement error. *British Medical Journal*, 313(7047), 41-42. <https://doi.org/10.1136/bmj.313.7048.41>.
- Bogaard, T. A., & Greco, R. (2018). Hydrological perspectives on precipitation intensity-duration thresholds for a landslide initiation: proposing hydro-meteorological thresholds. *Natural Hazards and Earth System Sciences*, 18(1), 31-39. <https://doi.org/10.5194/nhess-18-31-2018>.



- Brunetti, M. T., Peruccacci, S., Rossi, M., Luciani, S., Valigi, D., & Guzzetti, F. (2010). Rainfall thresholds for the possible occurrence of landslides in Italy. *Natural Hazards and Earth System Sciences*, 10(3), 447-458. <https://doi.org/10.5194/nhess-10-447-2010>.
- Caine, N. (1980). The rainfall intensity-duration control of shallow landslides and debris flows. *Geografiska Annaler Series A, Physical Geography*, 62(1-2), 23-27. <https://doi.org/10.1080/04353676.1980.11879996>.
- Cao, Y., Yin, K., Alexander, D. E., & Zhou, C. (2016). Using an extreme learning machine to predict the displacement of step-like landslides in relation to controlling factors. *Landslides*, 13(4), 725-736. <https://doi.org/10.1007/s10346-015-0596-z>.
- Cao, Y., Yin, K., Zhou, C., & Ahmed, B. (2020). Establishment of landslide groundwater level prediction model based on GA-SVM and influencing factor analysis. *Sensors (Switzerland)*, 20(3), 845. <https://doi.org/10.3390/s20030845>.
- Chae, B. G., Park, H. J., Catani, F., Simoni, A., & Berti, M. (2017). Landslide prediction, monitoring and early warning: a concise review of state-of-the-art. *Geosciences Journal*, 21(6), 1033-1070. <https://doi.org/10.1007/s12303-017-0034-4>.
- Chen, G., Zhang, G., Lu, S., & Wang, X. (2018). An attempt to quantify the lag time of hydrodynamic action based on the long-term monitoring of a typical landslide, Three Gorges, China. *Mathematical Problems in Engineering*, 2018, 5958436. <https://doi.org/10.1155/2018/5958436>.
- Chhorn, C., Yune, C. Y., Kim, G., & Lee, S. W. (2016). Study for assessment of rainfall duration inducing landslides. *Proceedings of the Institution of Civil Engineers: Municipal Engineer*, 169(2), 100-108. <https://doi.org/10.1680/jmuen.14.00028>.
- Cho, S. E. (2017). Prediction of shallow landslide by surficial stability analysis considering rainfall infiltration. *Engineering Geology*, 231, 126-138. <https://doi.org/10.1016/j.enggeo.2017.10.018>.
- Chae, B. G., Wu, Y. H., Liu, K. F., Choi, J., & Park, H. J. (2020). Simulation of debris-flow runoff near a construction site in Korea. *Applied Sciences*, 10(17), 6079. <https://doi.org/10.3390/app10176079>.
- Cohen, E. R. (1998). An introduction to error analysis: The study of uncertainties in physical measurements. *Measurement Science and Technology*, 9(6), 022. <https://doi.org/10.1088/0957-0233/9/6/022>.
- Cruden, D. M. (1991). A simple definition of a landslide. *Bulletin of the International Association of Engineering Geology - Bulletin de l'Association Internationale de Géologie de l'Ingénieur*, 43(1), 27-29. <https://doi.org/10.1007/BF02590167>.
- Dal Seno, N., Evangelista, D., Piccolomini, E., & Berti, M. (2024). Comparative analysis of conventional and machine learning techniques for rainfall threshold evaluation under complex geological conditions. *Landslides*, 1-19. <https://doi.org/10.1007/s10346-024-02336-3>.
- Das, P., Patwa, D., & Bharat, T. V. (2022). Influencing factors on the simulation of rainfall-induced landslide prediction based on case study. *Bulletin of Engineering Geology and the Environment*, 81(5), 194. <https://doi.org/10.1007/s10064-022-02682-3>.
- Davar, S., Nobahar, M., Khan, M. S., & Amini, F. (2022). The development of PSO-ANN and BOA-ANN models for predicting matric suction in expansive clay soil. *Mathematics*, 10(16), 2825. <https://doi.org/10.3390/math10162825>.
- De Luca, D. L., & Versace, P. (2017). A comprehensive framework for empirical modeling of landslides induced by rainfall: the Generalized FLAIR Model (GFM). *Landslides*, 14(13), 1009-1030. <https://doi.org/10.1007/s10346-016-0768-5>.
- de Souza, F. T., & Ebecken, N. F. (2012). A data based model to predict landslide induced by rainfall in Rio de Janeiro city. *Geotechnical and Geological Engineering*, 30(1), 85-94. <https://doi.org/10.1007/s10706-011-9451-8>.
- Dou, J., Paudel, U., Oguchi, T., Uchiyama, S., & Hayakawa, Y. S. (2015). Shallow and deep-seated landslide differentiation using support vector machines: a case study of the Chuetsu Area, Japan. *TAO: Terrestrial, Atmospheric and Oceanic Sciences*, 26(2), 227-239. [https://doi.org/10.3319/TAO.2014.12.02.07\(EOSI\)](https://doi.org/10.3319/TAO.2014.12.02.07(EOSI)).
- Ebrahim, K. M. P., Gomaa, S. M. H., Zayed, T., & Alfalah, G. (2024a). Rainfall-induced landslide prediction models, part ii: deterministic physical and phenomenologically models. *Bulletin of Engineering Geology and the Environment*, 83(3), 85. <https://doi.org/10.1007/s10064-024-03563-7>.
- Ebrahim, K. M. P., Fares, A., Faris, N., & Zayed, T. (2024b). Exploring time series models for landslide prediction: a literature review. *Geoenvironmental Disasters*, 11(1), 25. <https://doi.org/10.1186/s40677-024-00288-3>.



- Ebrahim, K. M. P., Gomaa, S. M. M. H., Zayed, T., & Alfalah, G. (2024c). Recent Phenomenal and Investigational Subsurface Landslide Monitoring Techniques: A Mixed Review. *Remote Sensing*, 16(2), 385. <https://doi.org/10.3390/rs16020385>
- Ebrahim, K. M. P., & Zayed, T. (2024). Factors controlling the triggering randomness for rainfall-induced landslides. In Proceedings of the 18th African Regional Conference on Soil Mechanics and Geotechnical Engineering (ISSMGE), Algiers, Algeria, 6-9 October 2024
- Ering, P., & Babu, G. S. (2020). Characterization of critical rainfall for slopes prone to rainfall-induced landslides. *Natural Hazards Review*, 21(3), 06020003. [https://doi.org/10.1061/\(ASCE\)NH.1527-6996.0000385](https://doi.org/10.1061/(ASCE)NH.1527-6996.0000385).
- Formetta, G., & Capparelli, G. (2019). Quantifying the three-dimensional effects of anisotropic soil horizons on hillslope hydrology and stability. *Journal of Hydrology*, 570, 329-342. <https://doi.org/10.1016/j.jhydrol.2018.12.064>.
- Froude, M. J., & Petley, D. N. (2018). Global fatal landslide occurrence from 2004 to 2016. *Natural Hazards and Earth System Sciences*, 18(8), 2161-2181. <https://doi.org/10.5194/nhess-18-2161-2018>.
- Gao, W., Dai, S., & Chen, X. (2020). Landslide prediction based on a combination intelligent method using the GM and ENN: Two cases of landslides in the Three Gorges Reservoir, China. *Landslides*, 17(1), 111-126. <https://doi.org/10.1007/s10346-019-01273-w>.
- Gariano, S. L., Sarkar, R., Dikshit, A., Dorji, K., Brunetti, M. T., Peruccacci, S., & Melillo, M. (2019). Automatic calculation of rainfall thresholds for landslide occurrence in Chukha Dzongkhag, Bhutan. *Bulletin of Engineering Geology and the Environment*, 78(6), 4325-4332. <https://doi.org/10.1007/s10064-018-1415-2>.
- Guzzetti, F., Melillo, M. & Mondini, A.C. (2024). Landslide predictions through combined rainfall threshold models. *Landslides*. <https://doi.org/10.1007/s10346-024-02340-7>
- Han, H., Shi, B., & Zhang, L. (2021). Prediction of landslide sharp increase displacement by SVM with considering hysteresis of groundwater change. *Engineering Geology*, 280, 105876. <https://doi.org/10.1016/j.enggeo.2020.105876>.
- Harsa, H., Anistia, M. H., Mulsandi, A., Supriyadi, B., Kurniawan, R., Habibie, M. N., ... & Praja, A. S. (2023). Machine learning and artificial intelligence models development in rainfall-induced landslide prediction. *IAES International Journal of Artificial Intelligence*, 12(1), 262. <https://doi.org/10.11591/ijai.v12.i1.pp262-270>
- Ho, J. Y., & Lee, K. T. (2017). Performance evaluation of a physically based model for shallow landslide prediction. *Landslides*, 14(3), 961-980. <https://doi.org/10.1007/s10346-016-0762-y>.
- Ho, J. Y., Lee, K. T., Chang, T. C., Wang, Z. Y., & Liao, Y. H. (2012). Influences of spatial distribution of soil thickness on shallow landslide prediction. *Engineering Geology*, 124(1), 38-46. <https://doi.org/10.1016/j.enggeo.2011.09.013>.
- Hong, M., Kim, J., & Jeong, S. (2018). Rainfall intensity-duration thresholds for landslide prediction in South Korea by considering the effects of antecedent rainfall. *Landslides*, 15(3), 523-534. <https://doi.org/10.1007/s10346-017-0892-x>.
- Hong, Y., Adler, R., & Huffman, G. (2006). Evaluation of the potential of NASA multi-satellite precipitation analysis in global landslide hazard assessment. *Geophysical Research Letters*, 33(22), L22402. <https://doi.org/10.1029/2006GL028010>.
- Huang, J., Ju, N. P., Liao, Y. J., & Liu, D. D. (2015). Determination of rainfall thresholds for shallow landslides by a probabilistic and empirical method. *Natural Hazards and Earth System Sciences*, 15(12), 2715-2723. <https://doi.org/10.5194/nhess-15-2715-2015>.
- Huang, J., Wu, X., Ling, S., Li, X., Wu, Y., Peng, L., & He, Z. (2022). A bibliometric and content analysis of research trends on GIS-based landslide susceptibility from 2001 to 2020. *Environmental Science and Pollution Research*, 29(58), 86954-86993. <https://doi.org/10.1007/s11356-022-23732-z>.
- Huang, Y., & He, Z. (2023). Rainfall-oriented resilient design for slope system: Resilience-enhancing strategies. *Soils and Foundations*, 63(2), 101297. <https://doi.org/10.1016/j.sandf.2023.101297>.
- Hungry, O., Leroueil, S., & Picarelli, L. (2014). The Varnes classification of landslide types, an update. *Landslides*, 11(2), 167-194. <https://doi.org/10.1007/s10346-013-0436-y>
- Hussein, M., & Zayed, T. (2021). Crane operations and planning in modular integrated construction: Mixed review of literature. *Automation in Construction*, 122, 103466. <https://doi.org/10.1016/j.autcon.2020.103466>.
- Ji, J., Cui, H., Zhang, T., Song, J., & Gao, Y. (2022). A GIS-based tool for probabilistic physical modelling and prediction of landslides: GIS-FORM landslide susceptibility analysis in seismic areas. *Landslides*, 19(9), 2213-2231. <https://doi.org/10.1007/s10346-022-01885-9>.



- Kirkby, M. J. (1975). Hydrograph modeling strategies. *Process in Physical and Human Geography*, 69-90.
- Krkač, M., Bernat Gazibara, S., Arbanas, Ž., Sečanj, M., & Mihalić Arbanas, S. (2020). A comparative study of random forests and multiple linear regression in the prediction of landslide velocity. *Landslides*, 17(11), 2515-2531. <https://doi.org/10.1007/s10346-020-01476-6>.
- Krkač, M., Špoljarić, D., Bernat, S., & Arbanas, S. M. (2017). Method for prediction of landslide movements based on random forests. *Landslides*, 14(3), 947-960. <https://doi.org/10.1007/s10346-016-0761-z>.
- Lee, K. T., & Ho, J. Y. (2009). Prediction of landslide occurrence based on slope-instability analysis and hydrological model simulation. *Journal of Hydrology*, 375(3-4), 489-497. <https://doi.org/10.1016/j.jhydrol.2009.06.053>.
- Lee, M. L., Ng, K. Y., Huang, Y. F., & Li, W. C. (2014). Rainfall-induced landslides in Hulu Kelang area, Malaysia. *Natural Hazards*, 70(1), 353-375. <https://doi.org/10.1007/s11069-013-0814-8>.
- Li, Z., Cheng, P., & Zheng, J. (2021). Prediction of time to slope failure based on a new model. *Bulletin of Engineering Geology and the Environment*, 80(7), 5279-5291. <https://doi.org/10.1007/s10064-021-02234-1>.
- Lian, C., Chen, C. P., Zeng, Z., Yao, W., & Tang, H. (2016). Prediction intervals for landslide displacement based on switched neural networks. *IEEE Transactions on Reliability*, 65(3), 1483-1495. <https://doi.org/10.1109/TR.2016.2570540>.
- Lian, C., Zeng, Z., Yao, W., & Tang, H. (2014). Extreme learning machine for the displacement prediction of landslide under rainfall and reservoir level. *Stochastic Environmental Research and Risk Assessment*, 28(8), 1957-1972. <https://doi.org/10.1007/s00477-014-0875-6>.
- Liang, W. L., & Uchida, T. (2022). Performance and topographic preferences of dynamic and steady models for shallow landslide prediction in a small catchment. *Landslides*, 19(1), 51-66. <https://doi.org/10.1007/s10346-021-01771-w>.
- AECOM Asia Company Limited (2019). Detailed Study of the 29 August 2018 Landslides on the Natural Hillside above Fan Kam Road, Pat Heung. *Geotechnical Engineering Office, Hong Kong*, 363, 11.
- Liu, Q., Jian, W., & Nie, W. (2021). Rainstorm-induced landslides early warning system in mountainous cities based on groundwater level change fast prediction. *Sustainable Cities and Society*, 69, 102817.
- Liu, X., Wang, Y., Koo, R. C., & Kwan, J. S. (2022). Development of a slope digital twin for predicting temporal variation of rainfall-induced slope instability using past slope performance records and monitoring data. *Engineering Geology*, 308, 106825. <https://doi.org/10.1016/j.enggeo.2022.106825>.
- Liu, Y., Liu, D., Qin, Z., Liu, F., & Liu, L. (2016). Rainfall data feature extraction and its verification in displacement prediction of Baishuihe landslide in China. *Bulletin of Engineering Geology and the Environment*, 75(3), 897-907. <https://doi.org/10.1007/s10064-015-0847-1>.
- Long, J., Li, C., Liu, Y., Feng, P., & Zuo, Q. (2022). A multi-feature fusion transfer learning method for displacement prediction of rainfall reservoir-induced landslide with step-like deformation characteristics. *Engineering Geology*, 297, 106494. <https://doi.org/10.1016/j.enggeo.2021.106494>.
- Ma, J., Tang, H., Hu, X., Bobet, A., Zhang, M., Zhu, T., Song, Y., & Ez Eldin, M. A. M. (2017). Identification of causal factors for the Majiagou landslide using modern data mining methods. *Landslides*, 14(1), 311-322. <https://doi.org/10.1007/s10346-016-0693-7>.
- Yanbin M, Hongrui L, Lin W, Wengang Z, Zhengwei Z, Haiqing Y, Luqi W, Xingzhong Y. (2022). Machine learning algorithms and techniques for landslide susceptibility investigation: A literature review. *Tumu yu Huanjing Gongcheng Xuebao/Journal of Civil and Environmental Engineering*, 44 (1), 53-67. <https://doi.org/10.11835/j.issn.2096-6717.2021.102>.
- Marrapu, B. M., Kukunuri, A., & Jakka, R. S. (2021). Improvement in prediction of slope stability & relative importance factors using ANN. *Geotechnical and Geological Engineering*, 39(8), 5879-5894. <https://doi.org/10.1007/s10706-021-01872-2>.
- Melillo, M., Brunetti, M. T., Peruccacci, S., Gariano, S. L., Roccati, A., & Guzzetti, F. (2018). A tool for the automatic calculation of rainfall thresholds for landslide occurrence. *Environmental Modelling and Software*, 105, 230-243. <https://doi.org/10.1016/j.envsoft.2018.03.024>.
- Merghadi, A., Yunus, A. P., Dou, J., Whiteley, J., ThaiPham, B., Bui, D. T., Avtar, R., & Abderrahmane, B. (2020). Machine learning methods for landslide susceptibility studies: A comparative overview of algorithm performance. *Earth-Science Reviews*, 207, 103225. <https://doi.org/10.1016/j.earscirev.2020.103225>.
- Moher, D., Liberati, A., Tetzlaff, J., Altman, D. G., & PRISMA Group*. (2009). Preferred reporting items for systematic reviews and meta-analyses: the PRISMA statement. *Journal of Clinical Epidemiology*, 62(10), 1006-1012. <https://doi.org/10.1016/j.jclinepi.2009.06.005>.



- Neaupane, K. M., & Achet, S. H. (2004). Use of backpropagation neural network for landslide monitoring: a case study in the higher Himalaya. *Engineering Geology*, 74(3-4), 213-226. <https://doi.org/10.1016/j.enggeo.2004.03.010>.
- Niu, X., Ma, J., Wang, Y., Zhang, J., Chen, H., & Tang, H. (2021). A novel decomposition-ensemble learning model based on ensemble empirical mode decomposition and recurrent neural network for landslide displacement prediction. *Applied Sciences (Switzerland)*, 11(10), 4684. <https://doi.org/10.3390/app11104684>.
- Ng, C. W. W., Usman, M., & Guo, H. (2023). Spatiotemporal pore-water pressure prediction using multi-input long short-term memory. *Engineering Geology*, 322, 107194. <https://doi.org/10.1016/j.enggeo.2023.107194>
- Oguz, E. A., Depina, I., & Thakur, V. (2022). Effects of soil heterogeneity on susceptibility of shallow landslides. *Landslides*, 19(1), 67-83. <https://doi.org/10.1007/s10346-021-01738-x>.
- Oh, H. J., & Lee, S. (2017). Shallow landslide susceptibility modeling using the data mining models artificial neural network and boosted tree. *Applied Sciences (Switzerland)*, 7(10), 1000. <https://doi.org/10.3390/app7101000>.
- Pagano, L., Picarelli, L., Rianna, G., & Urciuoli, G. (2010). A simple numerical procedure for timely prediction of precipitation-induced landslides in unsaturated pyroclastic soils. *Landslides*, 7(3), 273-289. <https://doi.org/10.1007/s10346-010-0216-x>.
- Perrin, C., Michel, C., & Andréassian, V. (2003). Improvement of a parsimonious model for streamflow simulation. *Journal of Hydrology*, 279(1-4), 275-289. [https://doi.org/10.1016/S0022-1694\(03\)00225-7](https://doi.org/10.1016/S0022-1694(03)00225-7).
- Peruccacci, S., Brunetti, M. T., Gariano, S. L., Melillo, M., Rossi, M., & Guzzetti, F. (2017). Rainfall thresholds for possible landslide occurrence in Italy. *Geomorphology*, 290, 39-57. <https://doi.org/10.1016/j.geomorph.2017.03.031>.
- Petrucci, O. (2022). Landslide fatality occurrence: a systematic review of research published between January 2010 and March 2022. *Sustainability (Switzerland)*, 14(15), 9346. <https://doi.org/10.3390/su14159346>.
- Rodrigues Neto, J. M. D. S., Bhandary, N. P., & Fujita, Y. (2023). An Analytical Study on Soil Water Index (SWI), Landslide Prediction and Other Related Factors Using XRAIN Data during the July 2018 Heavy Rain Disasters in Hiroshima, Japan. *Geotechnics*, 3(3), 686-699. <https://doi.org/10.3390/geotechnics3030037>
- Saadatkhan, N., Kassim, A., & Lee, L. M. (2015). Hulu Kelang, Malaysia regional mapping of rainfall-induced landslides using TRIGRS model. *Arabian Journal of Geosciences*, 8(5), 3183-3194. <https://doi.org/10.1007/s12517-014-1410-2>.
- Sasahara, K. (2017). Prediction of the shear deformation of a sandy model slope generated by rainfall based on the monitoring of the shear strain and the pore pressure in the slope. *Engineering Geology*, 224, 75-86. <https://doi.org/10.1016/j.enggeo.2017.05.003>.
- Segoni, S., Piciullo, L., & Gariano, S. L. (2018). A review of the recent literature on rainfall thresholds for landslide occurrence. *Landslides*, 15(8), 1483-1501. <https://doi.org/10.1007/s10346-018-0966-4>.
- Shano, L., Raghuvanshi, T. K., & Meten, M. (2020). Landslide susceptibility evaluation and hazard zonation techniques—a review. *Geoenvironmental Disasters*, 7(1), 18. <https://doi.org/10.1186/s40677-020-00152-0>.
- Shentu, N., Yang, J., Li, Q., Qiu, G., & Wang, F. (2022). Research on the Landslide Prediction Based on the Dual Mutual-Inductance Deep Displacement 3D Measuring Sensor. *Applied Sciences (Switzerland)*, 13(1), 213. <https://doi.org/10.3390/app13010213>.
- Soga, K., Alonso, E., Yerro, A., Kumar, K., & Bandara, S. (2016). Trends in large-deformation analysis of landslide mass movements with particular emphasis on the material point method. *Géotechnique*, 66(3), 248-273. <https://doi.org/10.1680/jgeot.15.LM.005>
- Tengtrairat, N., Woo, W. L., Parathai, P., Aryupong, C., Jitsangiam, P., & Rinchumphu, D. (2021). Automated landslide-risk prediction using web gis and machine learning models. *Sensors (Switzerland)*, 21(13), 4620. <https://doi.org/10.3390/s21134620>.
- Thang, N. V., Wakai, A., Sato, G., Viet, T. T., & Kitamura, N. (2022). Simple Method for Shallow Landslide Prediction Based on Wide-Area Terrain Analysis Incorporated with Surface and Subsurface Flows. *Natural Hazards Review*, 23(4), 04022028. [https://doi.org/10.1061/\(ASCE\)NH.1527-6996.0000578](https://doi.org/10.1061/(ASCE)NH.1527-6996.0000578).
- Uwihirwe, J., Hrachowitz, M., & Bogaard, T. A. (2020). Landslide precipitation thresholds in Rwanda. *Landslides*, 17(10), 2469-2481. <https://doi.org/10.1007/s10346-020-01457-9>.
- Valentino, R., Meisina, C., Montrasio, L., Losi, G. L., & Zizioli, D. (2014). Predictive power evaluation of a physically based model for shallow landslides in the area of Oltrepò Pavese, Northern Italy. *Geotechnical and Geological Engineering*, 32(4), 783-805. <https://doi.org/10.1007/s10706-014-9758-3>.



- Van Eck, N., & Waltman, L. (2010). Software survey: VOSviewer, a computer program for bibliometric mapping. *Scientometrics*, 84(2), 523-538. <https://doi.org/10.1007/s11192-009-0146-3>.
- Vung, D. V., Tran, T. V., Ha, N. D., Duong, N. H. (2023). Advancements, Challenges, and Future Directions in Rainfall-Induced Landslide Prediction: A Comprehensive Review. *Journal of Engineering & Technological Sciences*, 55(4), 466-477. <https://doi.org/10.5614/j.eng.technol.sci.2023.55.4.9>
- Wang, C., & Zhao, Y. (2023). Time Series Prediction Model of Landslide Displacement Using Mean-Based Low-Rank Autoregressive Tensor Completion. *Applied Sciences (Switzerland)*, 13(8), 5214. <https://doi.org/10.3390/app13085214>.
- Wang, H., Long, G., Shao, P., Lv, Y., Gan, F., & Liao, J. (2023b). A DES-BDNN based probabilistic forecasting approach for step-like landslide displacement. *Journal of Cleaner Production*, 394, 136281. <https://doi.org/10.1016/j.jclepro.2023.136281>.
- Wang, L., Yan, E., Wang, Y., Huang, S., & Liu, Y. (2016). Load-Unload Response Characteristics and Prediction of Reservoir Landslides. *Electronic Journal of Geotechnical Engineering*, 21(17), 5599-5608.
- Wang, R., Zhang, K., Wang, W., Meng, Y., Yang, L., & Huang, H. (2023a). Hydrodynamic landslide displacement prediction using combined extreme learning machine and random search support vector regression model. *European Journal of Environmental and Civil Engineering*, 27(6), 2345-2357. <https://doi.org/10.1080/19648189.2020.1754298>.
- Wang, S., Zhang, K., van Beek, L. P., Tian, X., & Bogaard, T. A. (2020). Physically-based landslide prediction over a large region: Scaling low-resolution hydrological model results for high-resolution slope stability assessment. *Environmental Modelling and Software*, 124, 104607. <https://doi.org/10.1016/j.envsoft.2019.104607>.
- Willmott, C. J., & Matsuura, K. (2005). Advantages of the mean absolute error (MAE) over the root mean square error (RMSE) in assessing average model performance. *Climate Research*, 30(1), 79-82. <https://doi.org/10.3354/cr030079>.
- Wohlin, C. (2014). Guidelines for snowballing in systematic literature studies and a replication in software engineering. *Proceedings of the 18th International Conference on Evaluation and Assessment in Software*, 1-10. <https://doi.org/10.1145/2601248.2601268>.
- Wu, L., Huang, R., & Li, X. (2020). Hydro-mechanical analysis of rainfall-induced landslides. *Springer Singapore*, 1-235. <https://doi.org/10.1007/978-981-15-0761-8>.
- Wu, Y. M., Lan, H. X., Gao, X., Li, L. P., & Yang, Z. H. (2015). A simplified physically based coupled rainfall threshold model for triggering landslides. *Engineering Geology*, 195, 63-69. <https://doi.org/10.1016/j.enggeo.2015.05.022>.
- Wuni, I. Y., & Shen, G. Q. (2020). Critical success factors for modular integrated construction projects: A review. *Building Research and Information*, 48(7), 763-784. <https://doi.org/10.1080/09613218.2019.1669009>.
- Xing, Y., Yue, J., & Chen, C. (2019). Interval estimation of landslide displacement prediction based on time series decomposition and long short-term memory network. *IEEE Access*, 8, 3187-3196. <https://doi.org/10.1109/ACCESS.2019.2961295>.
- Yang, S., Jin, A., Nie, W., Liu, C., & Li, Y. (2022). Research on SSA-LSTM-based slope monitoring and early warning model. *Sustainability (Switzerland)*, 14(16), 10246. <https://doi.org/10.3390/su141610246>.
- Yao, W., Zeng, Z., Lian, C., & Tang, H. (2015). Training enhanced reservoir computing predictor for landslide displacement. *Engineering Geology*, 188, 101-109, DOI: <https://doi.org/10.1016/j.enggeo.2014.11.008>.
- Ye S, Liu Y, Xie K, Wen C, Tian H-L, He J-B, Zhang W. (2024). Study on Landslide Displacement Prediction Considering Inducement under Composite Model Optimization. *Electronics*. 13(7), 1271. <https://doi.org/10.3390/electronics13071271>
- Yin, X., Liu, H., Chen, Y., & Al-Hussein, M. (2019). Building information modelling for off-site construction: Review and future directions. *Automation in Construction*, 101, 72-91. <https://doi.org/10.1016/j.autcon.2019.01.010>.
- Zhang, J., Tang, H., Tannant, D. D., Lin, C., Xia, D., Wang, Y., & Wang, Q. (2021b). A novel model for landslide displacement prediction based on EDR selection and multi-swarm intelligence optimization algorithm. *Sensors*, 21(24), 8352. <https://doi.org/10.3390/s21248352>.
- Zhang, L. L., Zhang, J., Zhang, L. M., & Tang, W. H. (2011). Stability analysis of rainfall-induced slope failure: a review. *Proceedings of the Institution of Civil Engineers-Geotechnical Engineering*, 164(5), 299-316. <https://doi.org/10.1680/jgeeng.2011.164.5.299>.



- Zhang, W., Goh, A. T., & Zhang, Y. (2016). Multivariate adaptive regression splines application for multivariate geotechnical problems with big data. *Geotechnical and Geological Engineering*, 34(1), 193-204. <https://doi.org/10.1007/s10706-015-9938-9>.
- Zhang, Y. G., Tang, J., Liao, R. P., Zhang, M. F., Zhang, Y., Wang, X. M., & Su, Z. Y. (2021a). Application of an enhanced BP neural network model with water cycle algorithm on landslide prediction. *Stochastic Environmental Research and Risk Assessment*, 35, 1273-1291. <https://doi.org/10.1007/s00477-020-01920-y>.
- Zhao, B., Dai, Q., Han, D., Dai, H., Mao, J., & Zhuo, L. (2019a). Probabilistic thresholds for landslides warning by integrating soil moisture conditions with rainfall thresholds. *Journal of Hydrology*, 574, 276-287. <https://doi.org/10.1016/j.jhydrol.2019.04.062>.
- Zhao, B., Dai, Q., Han, D., Dai, H., Mao, J., Zhuo, L., & Rong, G. (2019b). Estimation of soil moisture using modified antecedent precipitation index with application in landslide predictions. *Landslides*, 16(12), 2381-2393. <https://doi.org/10.1007/s10346-019-01255-y>.
- Zhao, B., Dai, Q., Han, D., Zhang, J., Zhuo, L., & Berti, M. (2020). Application of hydrological model simulations in landslide predictions. *Landslides*, 17(4), 877-891. <https://doi.org/10.1007/s10346-019-01296-3>.
- Zou, Y., & Zheng, C. (2022). A Scientometric analysis of predicting methods for identifying the environmental risks caused by landslides. *Applied Sciences (Switzerland)*, 12(9), 4333. <https://doi.org/10.3390/app12094333>.